Chemical Geology 183 (2002) 63–86

CHEMICAL GEOLOGY
INCLUDING
ISOTOPE GEOSCIENCE

www.elsevier.com/locate/chemgeo

Major to trace element analysis of melt inclusions by laser-ablation ICP-MS: methods of quantification

Werner E. Halter[a,*], Thomas Pettke[a], Christoph A. Heinrich[a], Barbara Rothen-Rutishauser[b]

[a]Isotope Geochemistry and Mineral Resources, Department of Earth Sciences, Swiss Federal Institute of Technology, ETH Zentrum NO, CH-8092 Zurich, Switzerland
[b]Institute of Pharmaceutical Sciences, Swiss Federal Institute of Technology, ETH Irchel, CH-8057 Zurich, Switzerland

Abstract

Current techniques for the quantification of melt inclusion chemistry require that inclusions are compositionally homogeneous and that post-entrapment devitrification or crystallization onto the inclusion walls could be reversed by appropriate re-melting. Laser-ablation ICP-MS provides a technique by which single heterogeneous inclusions can be analysed, thus avoiding the above prerequisites. Because host mineral is ablated with the inclusion, quantification of the melt composition necessitates deconvolution of the mixed signal by an internal standard. This can be obtained in various ways, including: (1) a fixed, pre-determined, concentration of a given element in the melt; (2) whole rock differentiation trends in a given igneous suite; (3) a constant, measured, distribution coefficient between the host and the inclusion melt and (4) determination of the volume ratios between the inclusion and total ablated volume. These four approaches were tested on a large set of cogenetic inclusions from a single plagioclase crystal in a rhyodacitic intrusion. Results suggest that quantification through whole rock differentiation trends is the most widely applicable, the most accurate and the least time-consuming technique, provided that the resulting data are critically interpreted with regard to the underlying assumptions. Uncertainties on the calculated element concentrations in the inclusions depend on the mass ratio between the melt inclusion and the host for a given ablation. They are of the order of 10% if the melt inclusion contributes more than 20% to the bulk analytical signal of a particular element. Calculated limits of detection for spherical 10 μm melt inclusions are of the order of a few ppm for elements strongly enriched in the melt relative to the host crystal. Concentrations in the melt inclusions can be determined even for elements enriched in the host mineral, but in this case uncertainties and calculated limits of detection increase with the concentration in the host. The uncertainty on the melt composition from a set of cogenetic inclusions can be commonly decreased by calculating of an uncertainty-weighted average of the concentration and their uncertainty.

Keywords: Melt inclusions; Laser ablation; ICP-MS; Composition; Quantification

1. Introduction

Since the first electron microprobe (EMP) analysis of melt inclusions (Clocchiatti, 1975), the study of these little droplets of melt (Fig. 1) has provided important insight into igneous processes. This motivated a search for new analytical tools, in particular for the analysis of trace elements. Secondary Ion microprobe Mass Spectrometry (SIMS) and Proton Induced X-ray Emission (PIXE) are two such tools

* Corresponding author.

PII: S0009-2541(01)00372-2

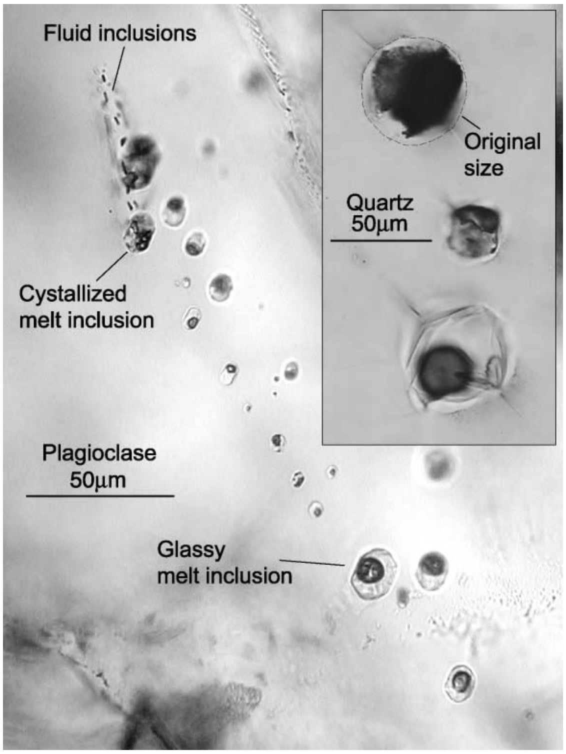

Fig. 1. Polyphase glassy and cystallized melt inclusions trapped on a growth zone of a plagioclase. In this case, crystallization of melt inclusions occurred as a result of re-opening and introduction of fluid (as apparent from the cross-cutting fluid inclusion trail). The inset shows inclusions in quartz with typical cracks at the inclusion tips and a clear halo probably representing the original inclusion size.

that have provided a growing number of high quality data in recent years (Webster and Duffield, 1991, 1994; Sobolev and Shimizu, 1993; Dietrich et al., 2000). Limitations of these techniques are that they can only be applied to homogeneous melt inclusions exposed to the sample surface (e.g., SIMS, EMP) or to inclusion in chemically simple host minerals (PIXE). Few inclusions fulfil these requirements a priori and all others need to be homogenized through heating to the trapping temperature.

An alternative technique for micro-analysis of major to trace elements is Laser-Ablation Inductively-Coupled-Plasma Mass-Spectrometry (LA-ICP-MS) and first analyses of melt inclusions with this technique have been acquired by Taylor et al. (1997) and Kamenetsky et al. (1998) on homogenized inclusions exposed to the sample surface. However, the major advantage of LA-ICP-MS is that bulk, multi-phase inclusions (melt or fluid) can be analysed up to 100 μm below the sample surface (Günther et al., 1998; Audétat et al., 1998; Ulrich et al., 1999). This avoids the prerequisite condition of homogeneity, and rules out the risk of decrepitation upon heating, especially of fluid-rich melt inclusions, and of inappropriate homogenisation temperatures that results in inadequate melting of the host mineral. Moreover, the time consuming step of bringing inclusions to the sample surface, thereby possibly losing a majority of inclusions in a given sample, is avoided. Recently, first attempts to analyse unexposed inclusions yielded some qualitative (Kamenetsky et al., 1999) and quantitative results (Audétat et al., 2000; Ulrich, 1999) for inclusions in quartz. Bulk analyses of inclusions in chemically more complex host minerals, e.g., in plagioclase, amphibole or pyroxene have not yet been quantified.

In this contribution, we provide a systematic tool for the analytical setup, data reduction and interpretation of LA-ICP-MS analysis of melt inclusions. Each unknown represents a sample volume of an ablation pit composed of host mineral only or of an entire inclusion plus some material from the host (Fig. 2). We then report the first quantitative analyses of bulk melt inclusions from a natural plagioclase using this technique, together with detection limits and uncertainties in the data.

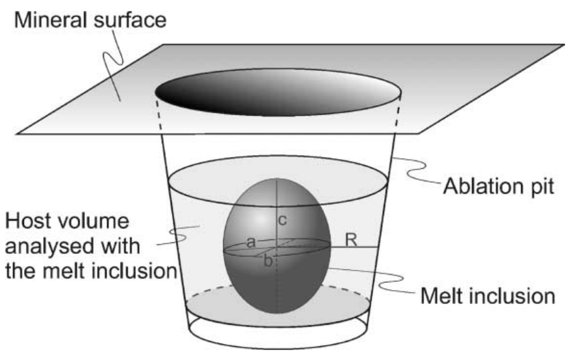

Fig. 2. Schematic representation of a melt inclusion and the ablation pit. The inclusion is approximated by an ellipsoid with its three axes a, b and c. The pit is approximated by a cylinder of radius R. The thickness of the host, which was ablated during the integration time, is taken to be the thickness $2c$ of the inclusion.

2. Analytical setup and sample description

2.1. Instrument parameters

Table 1 provides a compilation of instrument and data acquisition parameters. A pulsed 193 nm ArF Excimer laser with a homogenized beam profile was used (Günther et al., 1997). This system is characterized by a laterally homogeneous energy distribution, allowing depth-controlled ablation of material at a rate of 0.1–0.2 μm per shot, depending on laser energy and matrix chemistry. Moreover, a constant energy density over the entire pit area is a prerequisite for controlled ablation over variable pit sizes during crater drilling. Resulting ablation craters were nearly cylindrical and could be varied in diameter between 8 and 80 μm. The sample was loaded along with standards in a 1-cm^3 ablation cell and put on the table of a modified petrographic microscope. This enabled visual inspection of the ablation progress on a TV screen, essential for controlled sample ablation. If required, the pit size could be adjusted during analysis. Laser-ablation aerosol was carried to the ICP-MS by mixed He–Ar carrier gas (Günther and Heinrich, 1999). A quadrupole mass spectrometer was used for the analyses, the ELAN 6000, characterized by a linear dynamic range of up to nine orders of magnitude in dual detector mode. This enabled the measurement of matrix (up to 100 wt.%) to ultra-trace element concentrations ($\geq$ a few tens of ng g^{-1}) from the same sample in a single analysis.

Data acquisition is in sets of up to 20 individually stored runs whereby the two first and last analyses must be external standards which bracket up to 16 unknowns. The certified glass standards SRM 610 from NIST (hereafter NIST 610; Pearce et al., 1997) and BCR-2 g from USGS (Lahaye et al., 1997) were used for the experiments as external standards to calibrate analyte sensitivities. Typical dwell times (measurement times on each isotope during one quadrupole sweep) were set to 10 ms, the quadrupole settling time between measurements is 3 ms.

Table 1
LA-ICP-MS machine and data acquisition parameters

Excimer 193 nm ArF laser Compex 110I	
Output energy	Adjusted to between 180 and 240 mJ at 193 nm
Pulse duration	15 ns
Repetition rate	Adjusted to between 8 and 10 Hz
Pit size	Adjustable to between 8 and 80 μm
Ablation cell	Plexiglas with anti-reflection coated silica glass window
Cell He gas flow	Optimized to between 0.9 and 1.2 l min^{-1}
ELAN 6000 quadrupole ICP-MS	
Nebulizer gas flow	Optimized to between 0.95 and 1.20 l min^{-1} Ar
Auxiliary gas flow	Optimized to between 0.75 and 1.00 l min^{-1} Ar
Cool gas flow	Optimized to between 14.0 and 16.0 l min^{-1} Ar
rf Power	Optimized to between 1450 and 1550 kV
Detector mode	Dual, up to nine orders of magnitude linear dynamic range
Quadrupole settling time	3 ms
Detector housing vacuum	Between 1.5 and $2.8*10^{-5}$ Torr during analysis
Data acquisition parameters	
Sweeps per reading	1
Readings per replicate	Adjusted to between 200 and 1000 as a function of number of isotopes
Replicates	1
Dwell time per isotope	Adjusted to between 10 ms (standard) and 30 ms (to lower LOD)
Isotopes	^{23}Na, ^{25}Mg, ^{27}Al, ^{29}Si, ^{39}K, ^{42}Ca, ^{49}Ti, ^{55}Mn, ^{57}Fe, ^{65}Cu, ^{66}Zn, ^{85}Rb, ^{88}Sr, ^{89}Y, ^{90}Zr, ^{93}Nb, ^{133}Cs, ^{137}Ba, ^{139}La, ^{140}Ce, ^{146}Nd, ^{175}Lu, ^{208}Pb, ^{232}Th, ^{238}U

2.2. Sample description

The analytical and quantification methods are illustrated below, using 58 analyses of a suite of primary melt inclusions from a single plagioclase crystal (Fig. 1). The plagioclase comes from a rhyodacitic intrusion in the Farallon Negro Volcanic Complex (FNVC) in Northwestern Argentina. Its composition is approximately An_{33} and does not show any systematic variation from the core to the rim. This suggests that the melt, and thus the melt inclusions, should have similar compositions throughout the crystallization history of the plagioclase. Inclusions are either glassy with a large vapour bubble (approximately 20 vol.%) or re-crystallized (Fig. 1) and were expected to homogenize at temperatures between 800 and 900 °C. An attempt was made to homogenize inclusions in a similar crystal in an oven at various temperatures up to 1100 °C for 24 h, but, although the re-crystallized inclusions did melt, the vapour bubble in glassy and re-crystallized inclusion did not decrease in size.

3. Analytical results

Data were acquired in time-resolved signal mode, displayed on computer screen as signal intensity versus time plot with progressing analysis (Fig. 3). This enhanced the control on the sample ablation process. Each analysis started with monitoring of the gas blank for 20–30 s (segment 1 in Fig. 3). The first section of the ablation signal, until the melt inclusion is ablated, corresponds to pure host mineral (segment 2). As the inclusion is reached, mixed material from the host and the inclusion are analysed simultaneously in an unknown, evolving proportion (segment 3). After the entire inclusion is ablated (segment 4), element ratios are again identical to those of the pure host (segment 2) and the analysis is stopped. Data acquisition and reduction schemes followed recommendations given by Longerich et al. (1996) to calculate signal intensities (counts per second = cps) for the entire signal from a single ablation. The beginning and end of each signal interval is set manually and integrated over the corresponding time to give gross count rates. From the laser ablation

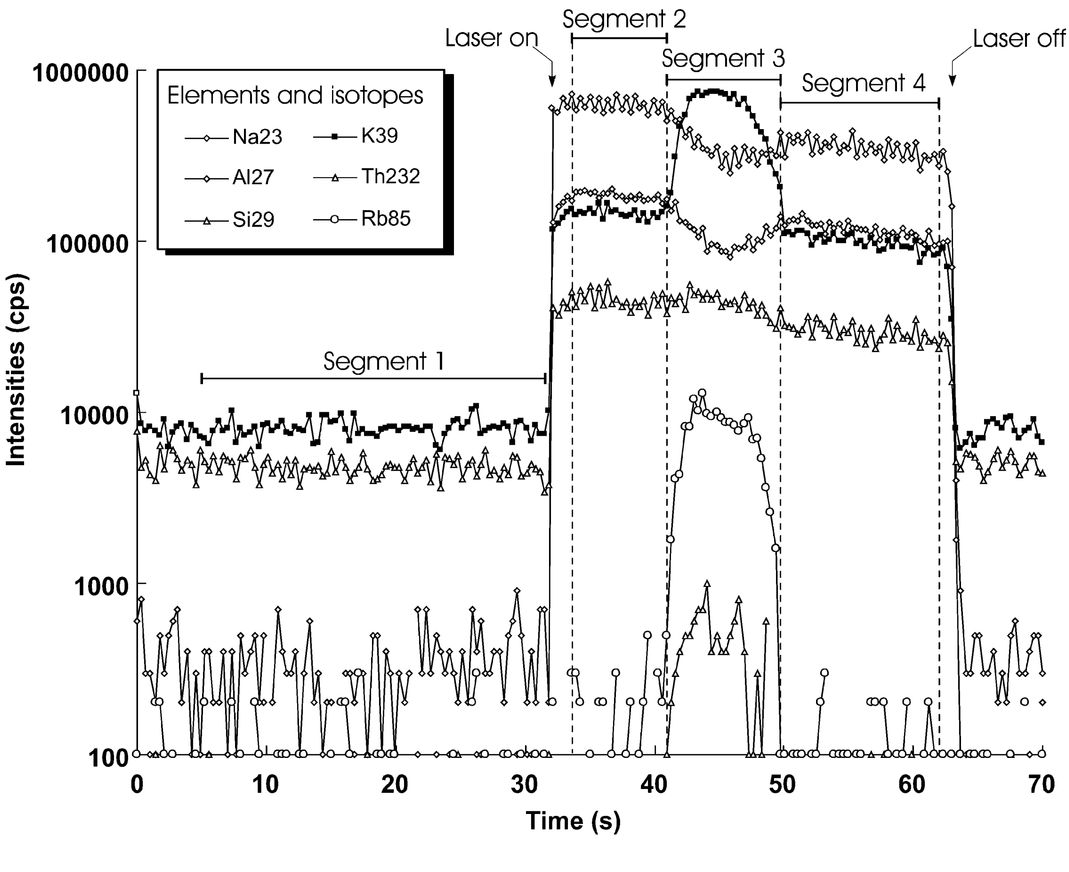

Fig. 3. Typical transient signal obtained from the ablation of a melt inclusion in plagioclase. Segment 1 is the gas background, segment 2, the interval during which the host mineral is ablated and segment 3 the interval during which the host and the inclusion are ablated together. Segment 4 is pure host ablation after having drilled through the inclusion.

signals (segments 2, 3 and 4) the corresponding gas background count rates determined on segment 1 are subtracted to give background corrected count rates.

4. Methods of quantification

The interpretation of the analytical signal into quantitative element concentrations in melt inclusions is the result of a three-step process. First, we need an expression to convert the analytical signal into element ratios through the use of an external standard. Element concentrations are then calculated by means of an internal standard. Finally, the host contribution to the element concentrations in the mixed host-melt signal (segment 3 in Fig. 3) has to be subtracted in order to obtain element concentrations in melt inclusions. These three steps are described below.

4.1. Determination of element ratios in the analyses

The mean signal intensities of the two first and the two last bracketing standards were used to correct linearly for instrumental drift during the acquisition of one sample set (16 unknowns). Drift-corrected signal intensities and the concentration in the standards were used to calculate sensitivity for each element individually, expressed as counts per unit time and concentration (cps/μg/g). Sensitivities depend on several factors including the ablation efficiency, ionisation efficiency and ion transmission. However, the ratio between the sensitivities of various elements is identical between measurements of the bracketing standards and unknowns, i.e., there is no ablation related change in the elemental ratios during the analyses (Fryer et al., 1995). Accordingly, we can determine element concentrations in the unknown as a function of a relative sensitivity factor, RSF, as

$$C_i^{\mathrm{SAMP}} = \frac{C_i^{\mathrm{STD}} \cdot I_i^{\mathrm{SAMP}}}{I_i^{\mathrm{STD}} \cdot \mathrm{RSF}} \tag{1a}$$

where C_i^{STD} is the concentration of an element i in the bracketing standard, I_i^{SAMP} is the intensity of an element i in the unknown, I_i^{STD} is the intensity of an element i in the bracketing standard, C_i^{SAMP} is the concentration of an element i in the unknown.

The RSF is identical for all the elements in one analysis. Hence, the ratios between element concentrations in the sample are uniquely determined even if the RSF is unknown.

4.2. Quantification of element concentrations in the analyses

An element for which the concentration in the sample $C_{\mathrm{is}}^{\mathrm{SAMP}}$ can be determined independently, is identified as a reference element or "internal standard" and establishes the RSF for each analysis by rearranging Eq. (1a)

$$\mathrm{RSF} = \frac{C_{\mathrm{is}}^{\mathrm{STD}} \cdot I_{\mathrm{is}}^{\mathrm{SAMP}}}{I_{\mathrm{is}}^{\mathrm{STD}} \cdot C_{\mathrm{is}}^{\mathrm{SAMP}}}. \tag{1b}$$

The concentration of all other elements is then obtained by Eq. (1a).

In the mixed signal (segment 3 in Fig. 3), the concentration of all elements changes with the host/melt ratio, hence no internal standard can be applied directly. To circumvent this problem, it can be assumed that the sum of the concentration of all the element oxides is 100% (or less if elements which cannot be analysed, like hydrogen, are present). This latter approach has been successfully applied to metal alloys (Leach and Hieftje, 2000) and results obtained in this study demonstrate, that it applies equally well to oxides (see evaluation of results below). We thus used this technique to determine the RSF in the mixed signal and the host. The host composition was obtained by integration of segment 2 where possible since the ablation efficiency is best in shallow pits, which allows more precise determination of element concentrations. If the inclusion was too close to the surface, segment 4 was used instead.

4.3. Element concentrations in melt inclusions

Quantification of element concentrations in melt inclusions requires that the relative contributions of inclusion and host to the mixed signal (segment 3 in Fig. 3) is known. These contributions can be represented by a mass ratio x, defined as the ratio of the mass of the inclusion over the total mass ablated during the time segment 3. So defined, x relates element concentrations in the host, the mixed signal and the inclusion as represented graphically in Fig. 4. From this figure, it is apparent that

$$x = \frac{m^{\mathrm{INCL}}}{m^{\mathrm{MIX}}} = \frac{C_i^{\mathrm{HOST}} - C_i^{\mathrm{MIX}}}{C_i^{\mathrm{HOST}} - C_i^{\mathrm{INCL}}} \qquad (2a)$$

where m refer to the masses of the inclusion and the total ablated mixture, and C_i^{HOST}, C_i^{MIX} and C_i^{INCL} are the concentrations of an element i in the host, in the mixture of host plus inclusion, and in the inclusion, respectively.

The mass ratio, x, can be determined in various ways, four of which are described below. In essence, we need to determine either the concentration of one element in the inclusion, or the masses of the inclusion and ablated material in the mix. Once this is done, x is uniquely defined and the concentration of all other elements, including elements present in the host mineral, can be determined by re-arranging Eq. (2a) into

$$C_i^{\mathrm{INCL}} = C_i^{\mathrm{HOST}} - \frac{(C_i^{\mathrm{HOST}} - C_i^{\mathrm{MIX}})}{x}. \qquad (2b)$$

In our example, results were then normalized to 96 wt.% as we assumed 4 wt.% of water in the melt according to volatile concentrations in melt inclusions of similar composition (Lowenstern, 1995). Iron was calculated as Fe_2O_3.

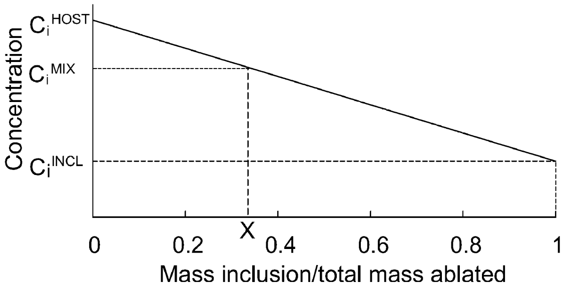

Fig. 4. Plot of the concentration C of an element i as a function of the mass ratio x between the inclusion and the total ablated material in the mixed signal section. C_i^{HOST}, C_i^{MIX} and C_i^{INCL} are the concentrations of an element i in the host (analysed), in the mixed signal of the host and the inclusion (analysed), and in the inclusion (extrapolated), respectively.

5. Determination of the mass ratio x

The following section describes four methods through which the ratio between the mass on the inclusion and the total mass ablated can be obtained. These methods are based on (1) a constant internal standard for the melt inclusion, (2) whole rock differentiation trends, (3) a constant distribution coefficient of an element between the host and the melt and (4) volume measurements of the inclusion and the ablated pit. Each method is characterized by various advantages/drawbacks.

5.1. Constant internal standard for the melt inclusion

Some elements vary little during igneous differentiation and can, to a first approximation, be taken as constant in a set of coeval melt inclusions. It is thus sufficient to estimate (from whole rock analyses) or to determine the absolute concentration of such an element in one of the melt inclusions and to take this concentration as an internal standard for the quantification of all coexisting inclusions. This is an attractive approach because, while the larger inclusions, providing enough material for analysis of trace elements, are generally difficult to homogenize, small inclusions are preserved in their glassy state or can be homogenized, thus allowing spot electron microprobe analyses of major elements (Audétat, 1999).

In the FNVC, this approach was tested using constant aluminium. Indeed, whole rock chemistry indicates that, in the entire igneous system, Al varies only between 17.4 and 14.0 wt.% from the early basalts to the late rhyolites (Sasso, 1997). The plagioclase used in this study comes from an evolved rhyodacite, and melt inclusions therein are likely to be even more differentiated than the whole rock. For a first approach to quantification, we thus selected an Al concentration of 14.0 wt.% as a constant internal standard for all the melt inclusions. The mass ratio for each inclusion was calculated using Eq. (2a). Values for x are given in Table 2.

The obvious shortcoming of this approach is twofold. First, a possible variability of the element which serves as an internal standard is neglected. Unrecognised variations of the internal standard yield incorrect values for x and, thus, for the concentrations of all the other elements. Second, x is best determined with

Table 2
Values for x calculated with different approaches

Incl.	Al	Diff.	DSr	Vol.	CM	1.6 CM
p4	0.12	0.12	0.24	0.07	0.05	0.09
p5	0.53	0.53	0.55	0.12	0.12	0.20
p6	0.07	0.07	0.19	0.06	0.04	0.06
p11	0.28	0.28	0.29	0.07		
p16	0.35	0.35	0.54	0.14		
p17	0.15	0.16	0.12	0.07		
p18	0.64	0.65	0.68	0.19		
p28	0.55	0.55	0.44	0.09		
p29	0.24	0.24	0.10	0.07		
p30	0.38	0.39	0.37	0.10		
p31R	0.50	0.50	0.44	0.16		
p32R	0.02	0.02	0.21	0.08		
p34	0.25	0.26	0.29	0.18		
p38	0.47	0.48	0.56	0.09		
p39	0.33	0.33	0.39	0.09		
p52	0.29	0.29	0.28	0.07		
p59	0.35	0.35	0.26	0.07		
p61	0.52	0.52	0.48	0.16		
p64R	0.40	0.40	0.37	0.14		
p68	0.59	0.60	0.45	0.21		
p69	0.39	0.39	0.35	0.15		
p71	0.70	0.71	0.75	0.31		
p72	0.40	0.40	0.35	0.15		
p73R	0.08	0.08	0.18	0.15	0.33	0.56
p74	0.41	0.41	0.31	0.15		
p75	0.38	0.38	0.41	0.18		
p77	0.10	0.10	0.13	0.10		
p78R	0.46	0.46	0.40	0.21		
p79R	0.04	0.05	0.04	0.21		
p87	0.34	0.34	0.32	0.15		
p88	0.45	0.46	0.47	0.25	0.28	0.48
p89	0.36	0.37	0.36	0.14		
p90R	0.20	0.20	0.26	0.14		
p91	0.27	0.27	0.19	0.05	0.13	0.23
p96	0.10	0.10	0.21	0.23		
p100R	0.61	0.61	0.56	0.23		
p102	0.23	0.23	0.18	0.09		
p104	0.41	0.42	0.43	0.09		
p105	0.37	0.44	0.36	0.34		
p106	0.11	0.12	0.26	0.29		
p107R	0.09	0.09	0.22	0.13		
p108	0.35	0.35	0.31	0.34		
p110	0.08	0.08	0.08	0.05		
p115R	0.07	0.07	0.11	0.08		
p116	0.31	0.32	0.35	0.11		
p117R	0.10	0.10	0.09	0.11		
p118	0.15	0.15	0.08	0.19		
p119R	0.29	0.30	0.21	0.21		
p120R	0.52	0.52	0.51	0.29		
p121R	0.50	0.50	0.53	0.18		
p124	0.24	0.01	0.24	0.15		
p125	0.01	0.01	0.09	0.12		
p126	0.20	0.20	0.19	0.07		
p128	0.06	0.06	0.17	0.13	0.24	0.41
p134R	0.41	0.41	0.39	0.07		
p137R	0.15	0.16	0.36	0.06		
p138R	0.15	0.15	0.35	0.12		

Qunatification methods: Al: fixed Al concentration at 14 wt.%; Diff.: Al and Fe correlation during differentiation; DSr: distribution coefficient of Sr as internal standard; Vol.: optical estimation of volume ratios; CM: volume estimation using confocal microscopy; 1.6 CM: volume ration as CM multiplied by 1.6.

highly compatible or highly incompatible elements (i.e., elements with concentrations much higher or much lower in the melt compared with the host crystal), as illustrated graphically in Fig. 5. Elements, which change little during differentiation do not fulfil this criterion and will inevitably result in a larger uncertainty on the value of x.

5.2. Whole rock differentiation trends

Bulk rock compositions of some magmatic suites indicate that the chemical evolution of the melt is dominated by differentiation processes. If the sample

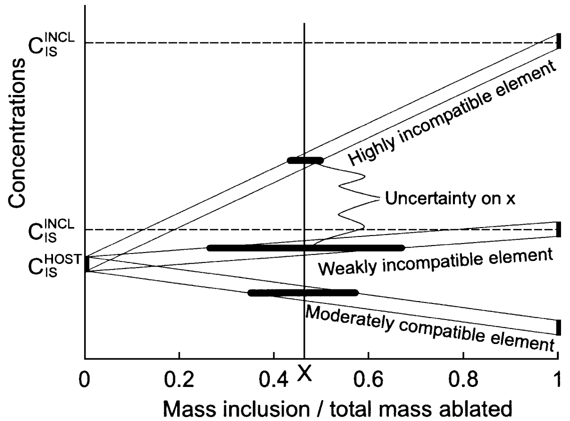

Fig. 5. Concentration versus x plot showing the importance of using highly incompatible (or compatible) elements to determine the mass ratio x. Given the same uncertainty on the analyses, the uncertainty on x is much larger if the difference in concentration of an element between host and inclusion is small. Indicated on the ordinate is the concentration of a reference element (the internal standard) in the inclusion C_{is}^{INCL} and in the host C_{is}^{HOST}.

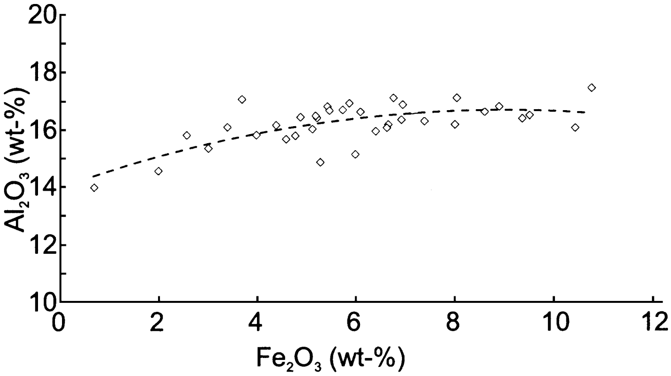

Fig. 6. Correlation between Fe_2O_3 and Al_2O_3 content of whole rocks in the Farallon Negro Volcanic complex. This correlation was used, together with Eq. (2b), to determine the mass factor x for each analysis individually.

considered is part of such a suite, the assumption of constant concentration of an element (e.g. Al) can be refined by using observed inter-element correlations. The assumption here is that, although two elements can vary significantly during the magmatic differentiation of a system, their relative concentrations follow a continuous evolution. For a given system, the correlation between two such elements in whole rocks is given by a function f

$$C_{\rm b} = f(C_{\rm a}). \tag{3}$$

From Eq. (2b), it is apparent that

$$C_{\rm a}^{\rm INCL} = C_{\rm a}^{\rm HOST} - \frac{(C_{\rm a}^{\rm HOST} - C_{\rm a}^{\rm MIX})}{x} \tag{4}$$

and

$$C_{\rm b}^{\rm INCL} = C_{\rm b}^{\rm HOST} - \frac{(C_{\rm b}^{\rm HOST} - C_{\rm b}^{\rm MIX})}{x}. \tag{5}$$

With the assumption that melts trapped in inclusions follow a similar differentiation trend as the whole rocks, we can calculate $C_{\rm a}^{\rm INCL}$, $C_{\rm b}^{\rm INCL}$ and x by combining Eqs. (4) and (5) with Eq. (3).

In the FNVC, whole rock chemistry indicates a tight negative correlation between the concentrations of Al and Fe (Fig. 6), which can be described with the function

$$C_{\rm Al} = -0.035 \cdot C_{\rm Fe}^2 - 0.624 \cdot C_{\rm Fe} + 13.89. \tag{6}$$

Values for $C_{\rm Al}^{\rm INCL}$ and $C_{\rm Fe}^{\rm INCL}$ in the inclusion were first calculated for $x = 0.5$ with Eqs. (4) and (5). The true value for x is the one satisfying Eq. (6). It can be calculated or obtained through iteration, depending on the form of the latter equation. The final results are given in Table 2 for comparison with the previous approach. It can be seen that values for x obtained with this approach do not differ significantly from those calculated using constant Al, reflecting the fact that Al in the melt remained essentially constant during the crystallization of this plagioclase. Other samples from the same rock suite show different Al concentrations and comparatively greater differences between these two approaches.

The differentiation approach for determining x has two advantages over that using a constant internal standard. First, inclusions can be quantified with one and the same function regardless of the degree of differentiation of the melt at the time the host mineral crystallized. Second, no measurements or assumptions on the concentration of the internal standard in the melt needs to be made.

5.3. Constant distribution coefficient of an element between mineral and melt

While absolute concentrations of all elements vary to different degrees during magmatic differentiation, distribution coefficients of trace elements between a mineral and the melt are either constant over a much wider compositional range, or can be predicted fairly reliably. The distribution coefficient, D_i, is defined by the relationship

$$C_i^{\mathrm{MIN}} = D_i \cdot C_i^{\mathrm{MELT}} \tag{7}$$

where C_i^{MIN} and C_i^{MELT} are the concentrations of an element i in the mineral and the melt, respectively. Thus, if the concentration of an element in the immediate host of an inclusion, C_i^{HOST} ($=C_i^{\mathrm{MIN}}$) and D_i are known, C_i^{MELT} (i.e., C_i^{INCL}) can be calculated for this inclusion and used as an internal standard in Eq. (2a). The distribution coefficient can be determined for the sample of interest using a few homogenized inclusions. Alternatively, D_i can be taken from the large dataset reported in the literature. Distribution coefficients vary to some degree as a function of P, T and bulk composition and care must be taken to select the most appropriate value from the literature.

In the sample from the FNVC, an average distribution coefficient D_{Sr} of 3.5 ± 1.0 for Sr between the plagioclase and the melt was obtained from LA-ICP-MS analyses of the largest inclusions (yielding the smallest uncertainty; see below). The Sr concentration of the host was determined for each run from segment 2 (Fig. 3). This value was used to calculate the Sr concentration for each inclusion individually and, in turn, x with Eq. (2a). Values for x obtained by this approach are reported in Table 2.

This method has several advantages. It explicitly accounts for variations in all elements from sample to sample, including the element used as an internal standard. More importantly, it is based on a quenched equilibrium between the melt inclusion and the immediate host mineral without any assumption about the entire magmatic system. This avoids the introduction of systematic uncertainties, for example, with melt inclusions in xenocrysts that are not directly related to the bulk composition of the enclosing magma (e.g., Dietrich et al., 2000). Finally, estimates of x with a small uncertainty can be obtained by using highly compatible or highly incompatible elements (Fig. 5).

Note that for the three methods described above no estimate of the amount of sidewall crystallization, nor accurate re-melting is required since the appropriate amount of host is added to the inclusion when the correct concentration in the internal standard is reached. In extreme cases, this can even yield values for x above 1, if the pit size is accidentally smaller than the original inclusion size.

5.4. Measuring volume ratios of ablated material and inclusion

The mass ratio x can also be calculated from measured volumes and the densities of the inclusion and the ablated host

$$x = \frac{m^{\mathrm{INCL}}}{m^{\mathrm{MIX}}} = \frac{V^{\mathrm{INCL}} \cdot \rho^{\mathrm{INCL}}}{V^{\mathrm{HOST}} \cdot \rho^{\mathrm{HOST}} + V^{\mathrm{INCL}} \cdot \rho^{\mathrm{INCL}}} \tag{8}$$

where V and ρ are the volume and the density of the inclusion and the host, respectively. The volume of the inclusion needs to be measured before the analysis. It should be remembered that in this case, the volume of the host mineral that crystallized from the melt onto the inclusion wall must be included in order to obtain the "true" volume of the inclusion. The volume of the ablated host is defined by the difference between the volume of the pit and the volume of the inclusion (Fig. 2).

In our example, the volume of each inclusion was approximated by an ellipsoid with two axes parallel to the sample surface. The pit was approximated by a cylinder with a diameter R and a height $2c$ equal to that of the inclusions (Fig. 2). This allows a simplification of Eq. (8) to

$$\begin{aligned} x &= \frac{\frac{4}{3}\pi abc\rho^{\mathrm{INCL}}}{\left(2c\pi R^2 - \frac{4}{3}\pi abc\right) \cdot \rho^{\mathrm{HOST}} + \frac{4}{3}\pi abc\rho^{\mathrm{INCL}}} \\ &= \frac{\frac{4}{3}\pi ab\rho^{\mathrm{INCL}}}{\left(2\pi R^2 - \frac{4}{3}\pi ab\right) \cdot \rho^{\mathrm{HOST}} + \frac{4}{3}\pi ab\rho^{\mathrm{INCL}}} \end{aligned} \tag{9}$$

Dimensions a and b (Fig. 2) were initially measured under a petrographic microscope. The radius R is the pit size selected during ablation. The densities ρ^{HOST} and ρ^{INCL} of the host plagioclase and the melt inclusion were taken to be 2.6 and 2.3, respectively. Values for x obtained with this method are compared to the previous results in Table 2.

The advantage over the previous methods is a total independence from any previous information or assumption on the melt chemistry or distribution coefficients. However, uncertainties associated with volume estimates may be considerable. To increase the accuracy of the method, the volumes of some inclusions were determined with the help of a Zeiss LSM 410 confocal microscope. This technique measures the intensity of light reflected from a surface, such as the wall of a melt inclusion. These intensities were visualized to a three-dimensional surface and integrated to yield the inclusion volume. This volume is smaller than the original inclusion volume since it does not include the shell of host mineral crystallized from the melt during cooling. In one case, the original volume could be recognized by a clear rim (without reflection of light) around the inclusion (see Fig. 1). In this example, the original volume was also determined and turned out to be approximately 1.6 times that of the present inclusion. Consequently, we multiplied all other inclusion volumes measured by confocal microscopy by a factor of two. The thickness $2c$ (Fig. 2) of the ablated cylinder was taken to be the thickness of the inclusion. Values for x calculated with these volume measurements are given in Table 2.

Note that, so far, we did not discuss changes in the ablation rate between the host and the mixture. Even though significant variations are expected (particularly for dark crystallized inclusions which may be ablated more rapidly, they will not affect the first three quantification methods, because they will only modify the mass factor x but none of the element ratios. However, the shape of the ablation pit might be affected by changes in the ablation rate, and a simple cylindrical geometry might deviate form the true geometry of the pit during ablation. This would results in an additional uncertainty on element concentrations determined with this approach.

6. Discussion of uncertainties and limits of detection

6.1. Uncertainties in the host and the mixture

As a first step to evaluate the overall uncertainty on each analysis, we repeatedly analysed a standard silicate glass (BCR-2g) with various pit diameters and depths (using NIST 610 as external standard), and quantified the signals using the total concentration of major elements as oxides (98.82 wt.% for the elements analysed). Results are shown in Table 3 and indicate that the reproducibility is generally within 5% (two standard deviations of 16 analyses).

The overall uncertainty at which the concentration of an element i can be determined in the host and the mixture from the laser-ablation measurement is the result of three independent contributions, namely (1) the uncertainty in the absolute number of counts as given by Poisson statistics, (2) the uncertainty due to noise in the ICP signal and (3) incomplete sampling of the time-restricted signal by the sequential quadrupole. The first two uncertainties are described below and were propagated in the calculation of the element concentrations in inclusions. The third contribution cannot be quantified for a single analysis, but is partly reflected in any scatter beyond the uncertainty in the calculated element concentrations in a suite of analyses of presumed isocompositional

Table 3
Repeated analyses of BCR-2g standard using the sum of oxides for quantification

	Average	Abs. Uncert.	Rel. Uncert. (%)
SiO_2	56.02	± 1.4	± 2.4
TiO_2	2.01	± 0.09	± 4.4
Al_2O_3	13.75	± 0.54	± 4.0
Fe_2O_3	11.75	± 0.28	± 2.4
MnO	0.19	± 0.006	± 2.8
MgO	3.34	± 0.16	± 5.0
CaO	6.80	± 0.44	± 6.6
Na_2O	3.26	± 0.17	± 5.4
K_2O	1.93	± 0.054	± 2.8
Pb	10.62	± 0.46	± 4.2
Zn	145.04	± 7.6	± 5.2
Nb	10.22	± 0.50	± 5.0
Y	29.56	± 2.4	± 8.2
Zr	159.61	± 13.8	± 8.8
U	1.69	± 0.09	± 5.6
Th	5.39	± 0.34	± 6.6
Cu	18.74	± 1.3	± 7.2
Ba	616.08	± 30	± 4.8
Rb	50.25	± 1.2	± 2.4
Sr	308.04	± 16.6	± 5.4
La	24.23	± 1.82	± 7.6
Ce	50.42	± 2.6	± 5.0
Cs	1.16	± 0.056	± 4.8
Nd	26.18	± 1.28	± 4.8
Lu	0.44	± 0.058	± 13.4

Uncertainties are one standard deviation of the signal.

inclusions. Note that for the present estimation of total uncertainty it is assumed that the element abundances of the external standard (i.e. BCR-2g) are known accurately. Reliable evaluations of the uncertainty in the standard composition are not available but are expected to be comparatively insignificant. Uncertainties due to polyatomic interferences or doubly charged ions were also considered negligible for this data set, but could be significant in some cases.

6.1.1. Uncertainties due to counting statistics, σ_p

The uncertainty, $\sigma_{p,i}$, on each determination of the numbers of counts of an element i follows a Poisson distribution and is thus given (in absolute cps) by

$$\sigma_{p,i} = \sqrt{n_i} \tag{10a}$$

where n_i is the absolute number of counts of an element i in one sweep

$$n_i = \frac{\text{cps} \cdot \text{dwell time}}{1000}. \tag{10b}$$

The dwell time is in milliseconds. During the analysis, n_i is determined N times, N being the number of sweeps in the integration interval. The absolute uncertainty on the analyses, i.e., on the integrated signal sections (Fig. 3), due to counting statistics, is thus

$$\frac{\sigma_{p,i}}{\sqrt{N}} \tag{10c}$$

and this applies to the background, the signal from the pure host and the signal from the mixture (the latter two not corrected for the background). Given that this uncertainty decreases with increasing n_i, its contribution to the overall uncertainty is only significant for a very small number of counts as in the background or for trace element signals.

6.1.2. Uncertainty due to noise in the ICP signal, σ_s

Due to instabilities in the plasma and to the short dwell times (10 ms) used to sample the signal properly, the recorded signals are not perfectly smooth. Individual intensity measurements during each sweep of the quadrupole fluctuate significantly, i.e., beyond counting statistics, around an average trend (Fig. 3). The deviation of each measurement from this trend is given by the relative standard deviation, $\sigma_{s,i}/I_i$, of the raw signal from an exponential function fitted through the data. In the host, values of $\sigma_{s,i}/I_i$ were determined for several elements with concentrations well above detection limits (i.e., were uncertainties due to counting statistics were insignificant). Results are plotted in Fig. 7 and suggest that, for a given dwell time, $\sigma_{s,i}/I_i$ deceases with signal intensity I_i, but is

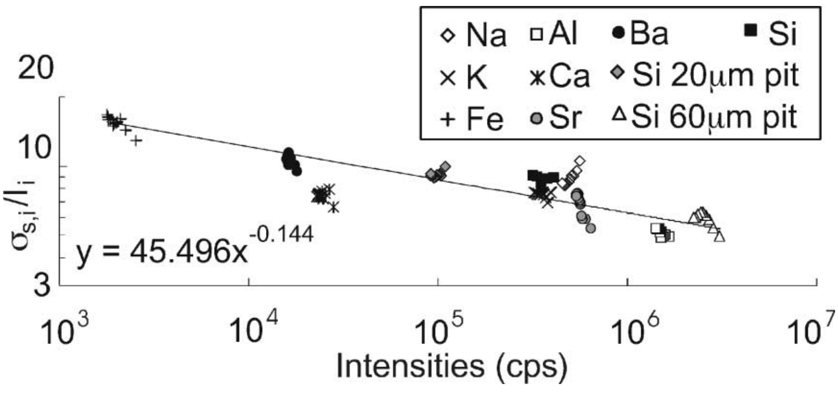

Fig. 7. Relative standard deviation due to instability in the plasma, $\sigma_{s,i}/I_i$, of various elements as a function of signal intensity. Each data set for one element represents various integration times of the same signal. This plot suggests that, a good approximation, $\sigma_{s,i}/I_i$ is independent of the pit size (40 μm for most elements; 20, 40 and 60 μm for Si) and integration time (all elements measured with 10 ms dwell time). The function fitted through the data was used to determine $\sigma_{s,i}/I_i$ for all the elements in every segment of the analytical signal.

independent of the element, the pit size or the integration time. Although the origin of this decrease is unclear, this correlation can be used to evaluate $\sigma_{s,i}/I_i$ for each element in the host. We can expect the same function to hold true during the ablation of the inclusion, and thus, calculate $\sigma_{s,i}/I_i$ for the ablation segment of inclusion plus host mixture. Note that this function is dependent on the instrument parameters and needs to be determined for each analytical setup. The decrease in $\sigma_{s,i}/I_i$ with increasing dwell time follows a Poisson distribution, i.e., it decreases as a function of 1/(dwell time)^2.

As above, the absolute uncertainties in the integrated signals are given by $\sigma_{s,i}/\sqrt{N}$ for the background, the host and the mixed signal and these uncertainties can be propagated to an uncertainty estimate of the inclusion composition.

6.1.3. Uncertainty due to incomplete sampling, σ_c

Since quadrupole-based ICP-MS measurements for each element are sequential and correspond to a series of discrete sweeps, the transient signal is simply a curve connecting individual analytical points through time. For quantitative analyses it is assumed that the signal intensity can be interpolated between points, but the true intensity could deviate from this interpolation. The uncertainty associated with this incomplete sampling, $\sigma_{c,i}$, can be significant (Pettke et al., 2000), particularly for trace elements, and contributes to the observed variation in element concentrations between inclusions of the same composition. However, other factors affect this variation, precluding quantification of $\sigma_{c,i}$. Decreasing the sweep time (e.g., the number of elements) minimizes the contribution of this uncertainty to the total uncertainty since the true shape of the transient signal will be better resolved.

6.2. Uncertainty in element concentrations in the host and the mixed signal

Neglecting the uncertainty due to incomplete sampling, $\sigma_{c,i}$, the total uncertainty on the integrated signal (in absolute numbers of counts per seconds) is given by

$$\sigma_i^{\mathrm{SIG}^2} = \left(\frac{\sigma_{p,i}}{\sqrt{N}}\right)^2 + \left(\frac{\sigma_{s,i}}{\sqrt{N}}\right)^2 \tag{11}$$

which was applied to the ablation segments 2 and 3 (Fig. 3). Similarly, subtracting the background signal from the signals in segments 2 and 3 (Fig. 3) implies that the squares of the uncertainties on the calculated concentration of an element i in the host (σ_i^{HOST}) or the mixture (σ_i^{MIX}) are given by the sum of the squares of the uncertainties in the signals

$$\sigma_i^{\mathrm{HOST}^2} = \sigma_i^{\mathrm{SIG1}^2} + \sigma_i^{\mathrm{SIG2}^2} \tag{12}$$

and

$$\sigma_i^{\mathrm{MIX}^2} = \sigma_i^{\mathrm{SIG1}^2} + \sigma_i^{\mathrm{SIG3}^2} \tag{13}$$

were $\sigma_i^{\mathrm{SIG1-3}}$ are the uncertainties in the signals of segments 1 to 3, respectively (Fig. 3).

6.3. Uncertainty in single melt inclusion compositions

Element concentrations of pure melt inclusions are calculated with Eq. (2b), which combined with Eq. (1a), can be written as a function of intensities I

$$C_i^{\mathrm{INCL}} = \frac{C_i^{\mathrm{STD}}}{I_i^{\mathrm{STD}}} \cdot \left(\frac{I_i^{\mathrm{SIG2}} - I_i^{\mathrm{SIG1}}}{\mathrm{RSF}^{\mathrm{HOST}}} \cdot \left(1 - \frac{1}{x}\right) + \frac{I_i^{\mathrm{SIG3}} - I_i^{\mathrm{SIG1}}}{x \cdot \mathrm{RSF}^{\mathrm{MIX}}} \right) \tag{14}$$

where $I_i^{\mathrm{SIG1-3}}$ are the intensities (in cps) of the signals in the intervals 1 to 3, $\mathrm{RSF}^{\mathrm{HOST}}$ and $\mathrm{RSF}^{\mathrm{MIX}}$ are the relative sensitivity factors during the ablation of the host or the mixture, respectively.

According to Eq. (14), uncertainties in the calculated concentrations in the inclusion, σ_i^{INCL}, depend on uncertainties in the intensities $I_i^{\mathrm{SIG1-3}}$, as well as on the uncertainty on the mass ratio x. The latter cannot be evaluated systematically since x varies between analyses. However, for the first three quantification methods, we can approximate the uncertainty on x by the uncertainty on the calculated concentration of the internal standard. Since the latter uncertainty depends on the uncertainty on x itself, the system must be solved iteratively.

Uncertainty propagation implies that the uncertainty on element concentrations in the inclusion (σ_i^{INCL}) obtained from Eq. (14), is given by

$$\sigma_i^{\mathrm{INCL}^2} = \left(\frac{C_i^{\mathrm{STD}}}{I_i^{\mathrm{STD}}}\right)^2 \cdot \left\{ \sigma_i^{\mathrm{SIG2}^2} \cdot \left[\frac{1}{\mathrm{RSF}^{\mathrm{HOST}}} \cdot \left(1 - \frac{1}{x}\right)\right]^2 + \sigma_i^{\mathrm{SIG1}^2} \cdot \left[\frac{1}{\mathrm{RSF}^{\mathrm{HOST}}} \cdot \left(1 - \frac{1}{x}\right) + \frac{1}{x \cdot \mathrm{RSF}^{\mathrm{MIX}}}\right]^2 + \sigma_i^{\mathrm{SIG3}^2} \cdot \left[\frac{1}{x \cdot \mathrm{RSF}^{\mathrm{MIX}}}\right]^2 + \frac{\sigma_x^2}{x^4} \cdot \left[\frac{I_i^{\mathrm{SIG2}} - I_i^{\mathrm{SIG1}}}{\mathrm{RSF}^{\mathrm{HOST}}} - \frac{I_i^{\mathrm{SIG3}} - I_i^{\mathrm{SIG1}}}{\mathrm{RSF}^{\mathrm{MIX}}}\right]^2 \right\} \quad (15)$$

where σ_x is the absolute uncertainty on x.

Uncertainties calculated with Eq. (15) are given in Table 6 and visualized for SiO_2, Al_2O_3, K_2O and Sr in Fig. 8, where the concentrations in all individual inclusions (obtained with the differentiation trend method) are plotted as a function of x. As expected, uncertainties are larger if x is small, i.e., with a larger extrapolation. Consequently, variations in the calculated concentration of these elements are high when $x < 0.2$ and analyses are considered reliable only above this value. Thus, it is crucial for an accurate determination of the melt composition that this mass ratio is as large as possible. In general, large x values can be obtained with large inclusions, ideally bigger than 20 μm. Uncertainties in the melt inclusion composition quantified with the other approaches described above are given for one inclusion in Table 4.

6.4. Limit of detection

For any element i, the limit of detection, LOD_i (the lowest significant intensity at 99% confidence level), in the host and in the mixed signal can be calculated from the standard deviations of the background (i.e., due to counting statistics and instability of the plasma), the length of the signals and Eq. (1b) using the formula (Longerich et al., 1996)

$$\mathrm{LOD}_i^{\mathrm{HOST,MIX}} = 3 \cdot \sqrt{\sigma_{\mathrm{p},i}^2 + \sigma_{\mathrm{s},i}^2} \cdot \sqrt{\frac{1}{N^{\mathrm{BG}}} + \frac{1}{N^{\mathrm{HOST,MIX}}}} \quad (16)$$

where N^{BG} and $N^{\mathrm{HOST,\ MIX}}$ are the number of sweeps in segment 1 and 2 or 3, respectively.

Similarly, the "background" to the signal from the inclusion is the intensity contribution of the host to the mixed signal, which can be calculated through

$$I_{i,\mathrm{HOST}}^{\mathrm{SIG3}} = I_i^{\mathrm{SIG1}} + \left(I_i^{\mathrm{SIG2}} - I_i^{\mathrm{SIG1}}\right) \cdot \mathrm{RSF}^{\mathrm{MIX}} \cdot \frac{1 - x}{\mathrm{RSF}^{\mathrm{HOST}}}. \quad (17)$$

A contribution from the inclusion to the mixed signal is considered significant when it exceeds three times the uncertainty in the mixed signal, $\sigma_{i,\mathrm{HOST}}^{\mathrm{SIG3}}$, calculated by replacing I_i^{SIG3} with $I_{i,\mathrm{HOST}}^{\mathrm{SIG3}}$. The lowest detectable intensity contribution from the inclusion is obtained by dividing through the mass factor x. Accordingly, the $\mathrm{LOD}_i^{\mathrm{INCL}}$ is given by

$$\mathrm{LOD}_i^{\mathrm{INCL}} = \frac{3}{x} \cdot \sqrt{\sigma_i^{\mathrm{SIG1}^2} + \sigma_{i,\mathrm{HOST}}^{\mathrm{SIG3}^2}}. \quad (18)$$

Uncertainties, and thus LOD_i's are largely dependent on the optimisation of instrument parameters and the number of measurements of each element in the signal interval (for a given length of transient signal, this is a function of the number of elements analysed and the dwell time for each element). In this study, 25 light to heavy elements (Table 1) were analysed without preferential tuning for any element. The LOD_i values achieved in this set of analyses can be improved by reducing the number of elements in the menu or by mass-specific tuning of the system. The calculated LOD_i's for single melt inclusions are generally of the order of a few to a few tens of ppm for elements that are not present in the host in significant amounts. Highly compatible elements and major elements in

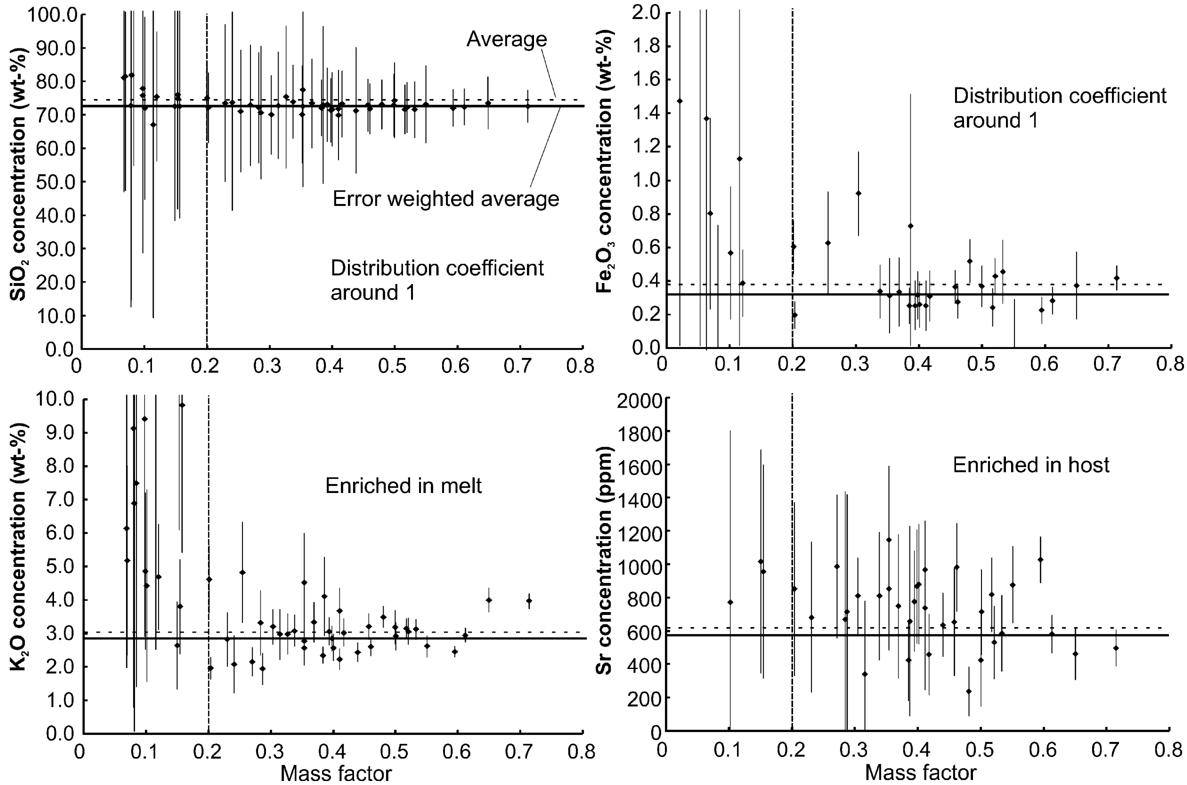

Fig. 8. Calculated SiO_2, Fe_2O_3, K_2O and Sr concentrations in all melt inclusions, with their 2σ uncertainties as a function of the mass factor x of the mixed signal. Uncertainties are large if x is small, and the concentrations are consistent above a value of approximately $x = 0.2$. Also shown are averages (dashed lines) and the uncertainty-weighted averages (solid lines). Regardless of the value of x, a large majority of the calculated concentrations overlap within their uncertainty with the average values.

the host have LOD_i's between a few hundreds of μg g^{-1} to a few percents.

7. Evaluation of results

From Table 2 it appears that values for x vary generally little between the various quantification approaches. As expected, the value obtained with the estimation of the volume ratios deviates most significantly form the others, unless volumes are measured with a confocal microscope and corrected for the crystallization of host onto the inclusion wall. Differences in melt compositions obtained with the various methods are often smaller than differences in x itself because variations in x affect only the concentration of highly compatible or incompatible elements. An example of this is given in Table 4, which shows the composition of a melt inclusion (p88) calculated with the various approaches.

Which of these methods yields the most accurate x value probably depends on the system under consideration. The most attractive technique is the one based on whole rock differentiation trends, and using this approach is recommended in systems evolving along simple trends. If two processes (e.g., mixing and fractionation) control chemical changes in the system, evolution might not follow such a simple trend and important information on magmatic processes, contained in melt inclusions, might be masked if this quantification technique is applied. In such cases, constant aluminium might be a useful alternative since this will visualise changes in elements with larger variations in the concentration than aluminium (i.e., most other elements). Absolute values for the concentrations are, however, more subject to a systematic

Table 4
Composition of inclusion p88 calculated with the various approaches to determine x

	Al	±2σ (%)	Diff.	±2σ (%)	DSr	±2σ (%)	Vol.	±2σ (%)	CM	±2σ (%)
x	0.45		0.46		0.47		0.25		0.48	
SiO_2	72.88	11	71.97	10	72.17	11	86.40	19	71.97	10
TiO_2	$0.01<I<0.02$	44	$0.01<I<0.02$	44	$0.01<I<0.02$	44	$0.02<I<0.03$	48	$0.01<I<0.02$	44
Al_2O_3	14.00	17	14.65	15	14.51	15	4.34	110	14.65	15
Fe_2O_3	0.36	28	0.35	27	0.35	27	0.54	38	0.35	27
MnO	0.02	20	0.02	19	0.02	19	0.03	25	0.02	19
MgO	0.03	103	0.03	99	0.03	100	< 0.06		0.03	99
CaO	< 1.17		< 1.08		< 1.10		ext. < 0		< 1.08	
Na_2O	4.97	12	5.06	11	5.04	11	3.65	34	5.06	11
K_2O	3.20	12	3.05	12	3.08	12	5.33	14	3.05	12
H_2O^a	4.00		4.00		4.00		4.00		4.00	
Total	99.47		99.14		99.21		104.29		99.14	
Cu	< LOD mix		< LOD mix		< LOD mix		< LOD mix		< LOD mix	
Zn	< LOD mix		< LOD mix		< LOD mix		< LOD mix		< LOD mix	
Rb	131.29	16	124.10	16	125.61	16	238.35	17	124.10	16
Sr	571.57	52	664.68	42	645.09	44	ext. < 0		664.68	42
Y	$7<I<8$	29	$7<I<7$	29	$7<I<7$	29	$12<I<14$	29	$7<I<7$	29
Zr	$39<I<40$	23	$37<I<38$	23	$37<I<39$	23	$70<I<74$	23	$37<I<38$	23
Nb	$8<I<9$	34	$8<I<9$	34	$8<I<9$	34	$14<I<17$	34	$8<I<9$	34
Cs	$6<I<6$	26	$5<I<6$	26	$5<I<6$	26	$10<I<11$	26	$5<I<6$	26
Ba	617.12	14	602.08	14	605.25	14	841.15	21	602.08	14
La	16.84	22	16.14	22	16.29	22	27.17	27	16.14	22
Ce	31.18	18	29.73	18	30.03	18	52.75	20	29.73	18
Nd	11.65	41	11.07	41	11.19	41	20.27	46	11.07	41
Lu	< 0.29		< 0.28		< 0.27		< 0.52		< 0.27	
Pb	11.74	43	11.74	40	11.74	41	11.70	92	11.74	40
Th	$4<I<4$	31	$3<I<4$	31	$4<I<4$	31	$6<I<7$	31	$3<I<4$	31
U	$0<I<1$	54	$0<I<1$	54	$0<I<1$	54	$1<I<1$	54	$0<I<1$	54

$5.77<I<6.00$: bracketing values.
< 0.83: below detection limit.
ext. < 0: calculated concentration below zero.
< LOD mix: below LOD in the mixed signal.
Abbreviations for the quantification methods as in Table 2.
H_2O^a estimated water content.

uncertainty with this approach. If accurate data on distribution coefficients are available, the third quantification method is certainly a valuable alternative to the previous two techniques but it has the disadvantage of being dependent on the host mineral.

In the present example, the first two approaches yield almost identical results (because the compositional range of the melt is very restricted). Melt inclusion compositions obtained with whole rock differentiation trends are given in Table 6 and the variability of the SiO_2, Fe_2O_3, K_2O and Sr concentrations are shown graphically in Fig. 8. Concentrations of elements below the LOD_i in the host are given as bracketed values (Tables 4 and 6): the maximum was calculated with a theoretical minimum concentration of 0 wt.% of the element in the host, the minimum with a concentration equal to the limit of detection in the host.

7.1. Average melt compositions derived from cogenetic melt inclusion populations

The compositions of melt the inclusions in our experiment do not vary systematically across the plagioclase crystal, justifying the calculation of average element concentrations in the melt from individual analyses. The most commonly used approach to calculate this mean is to simply average melt compositions, neglecting the uncertainties on the single inclusion determinations. This average (for analyses with $x>0.2$) is shown in Table 5, along with the associated two-sigma uncertainty, given by two standard deviations in calculated concentrations. Also shown are the median values, representing the most frequent concentrations in the set of inclusions.

A better estimate of the melt composition is obtained by weighting each point by its associated uncertainty (uncertainty-weighted average). This approach favours analyses with small uncertainties over imprecise results. Note that is can be used only to average data sets for internally homogeneous samples. It should not be applied to elements for which the real variability between single inclusions exceeds the associated uncertainty (e.g. K, Na, Rb in Fig. 8). Values for these elements are given in italics for reference only in Table 5. The uncertainty-weighted average, μ, is calculated as (e.g., Bevington and Robinson, 1992)

$$\mu = \frac{\sum C_i/\sigma_i^2}{\sum 1/\sigma_i^2} \tag{19}$$

where C_i is the concentration of an element, i, and σ_i its associated uncertainty. The uncertainty associated with this average is given by

$$\sigma_\mu^2 = \frac{1}{\sum 1/\sigma_i^2}. \tag{20}$$

Table 5 shows that the difference between averages and uncertainty-weighted averages can be significant and that the uncertainty on the uncertainty-weighted average is sometimes drastically reduced when compared to uncertainties on simple averages.

The mean square of weighted deviates (MSWD) gives a measure of the homogeneity of the population and is calculated through

$$\text{MSWD} = \frac{\sigma_i^{\text{EXT}^2}}{\sigma_\mu^2} \tag{21}$$

where ${\sigma_i}^{\text{EXT}}$ is the external uncertainties on i obtained by

$$\sigma_i^{\text{EXT}^2} = \frac{\sum (C_i-\mu)^2/\sigma_i^2}{(n-1)\cdot \sigma_\mu^2}. \tag{22}$$

Values for the MSWD, reported in Table 5, identify homogeneously distributed elements (MSWD is small) and element for which the inherent variation is larger than the uncertainty (MSWD ~ 3 or higher).

Variations exceeding the total calculated uncertainty of each analysis could be due to several causes. (1) Changes in the melt composition (boundary effects or changes in melt composition during growth of the plagioclase). No systematic changes in the composition of the inclusions from the core and the rim of the crystal was detected, but fluctuations are possible (the plagioclase is zoned). (2) Zonation of the host mineral phase and a resulting difference in the host composition between segments 2 and 3 (Fig. 3). The latter explanation is supported by the fact that the strongest variations are observed for concentrations of elements

Table 5
Average, median, uncertainty-weighted averages and mean square of weighted deviates (MSWD) of melt inclusion analyses

	Average	$\pm 2\sigma$ (%)	Median	UWA	$\pm 2\sigma$ (%)	MSWD
SiO_2	72.44	4.1	72.32	72.27	2.2	0.04
TiO_2	0.02	82	0.02	0.02	12	2.8
Al_2O_3	14.14	3.8	14.06	14.16	2.6	0.01
Fe_2O_3	0.38	92	0.33	0.32	8	2.7
MnO	0.02	73	0.02	*0.02*	*5*	6.2
MgO	0.05	95	0.04	0.04	23	0.8
CaO	2.19	54	2.12	1.77	18	1.5
Na_2O	4.60	50	4.75	*4.64*	*2.2*	9.8
K_2O	3.02	47	2.97	*2.83*	*2.1*	8.9
H_2O[a]	4.00		4.00	4.00		
Total	100.88		100.64	100.07		
Cu	25	[b]	25	25		
Zn	50	47	53	41	38	0.5
Rb	134	64	128	*118*	*3.4*	8.9
Sr	639	60	661	*576*	*6.4*	3.8
Y	5.5	76	5.5	4.5	10	2.5
Zr	43	81	39	*35*	*6*	5.3
Nb	8.9	103	7.8	*6.3*	*10*	4.3
Cs	6.1	105	5.0	*4.4*	*8*	5.5
Ba	456	78	434	*389*	*3.5*	14.5
La	12	74	11	10	6	4.3
Ce	21	70	20	*18*	*5*	7.2
Nd	10	91	10	8.0	15	1.5
Pb	19	71	17	16	7	1.9
Th	5.0	142	4.5	*3.5*	*8*	5.2
U	2.3	133	2.0	*1.2*	*11*	8.2

Major elements in wt.% oxides, trace elements in ppm.
UWA: uncertainty-weighted average.
$\pm 2\sigma$ of the average is the two standard deviation of the element concentrations.
$\pm 2\sigma$ of the UWA is twice the uncertainty calculated with Eq. (20).
[a] Assumed water content; see text.
[b] Cu was only detected once.

Table 6
Composition of melt inclusions obtained with the quantification through the fractionation trend and the calculated 2σ uncertainty

	p4		p5		p6		p11		p16		p17	
SiO_2	75.32	26%	71.43	12%	81.44	42%	72.04	23%	77.34	38%	74.65	25%
TiO_2	0.03	53%	0.03 < I < 0.03	55%	0.04	74%	0.01 < I < 0.02	97%	< LOD mix		0.02	74%
Al_2O_3	14.13	40%	14.17	12%	14.13	65%	14.03	38%	14.12	43%	14.04	49%
Fe_2O_3	0.38	53%	0.45	42%	< 0.39		< 0.31		< LOD mix		< 0.33	
MnO	0.04	37%	0.01	43%	0.04	61%	0.01	65%	< LOD mix		0.02	45%
MgO	0.04	86%	< LOD mix		< 0.05		< LOD mix		< LOD mix		< 0.05	
CaO	ext. < 0		2.83	49%	ext. < 0		< 3.16		ext. < 0		ext. < 0	
Na_2O	3.73	50%	3.99	13%	< 3.11		5.92	19%	2.00	72%	3.44	46%
K_2O	4.67	34%	3.09	10%	5.14	55%	3.28	30%	4.49	33%	3.77	38%
Total	98.34		95.97		100.79		95.29		97.95		95.95	
Cu	11 < I < 20	96%	< LOD mix		< LOD mix		< LOD mix		< LOD mix		< LOD mix	
Zn	< 39		< LOD mix		< 76		< LOD mix		< LOD mix		< LOD mix	
Rb	178	40%	152 < I < 153	17%	269	64%	164 < I < 167	38%	188 < I < 194	46%	174	45%
Sr	ext. < 0		525	39%	ext. < 0		600	115%	ext. < 0		860	67%
Y	10	46%	8 < I < 8	47%	11 < I < 12	71%	5 < I < 6	68%	18 < I < 19	90%	8 < I < 10	59%
Zr	64 < I << I < 65	42%	32 < I < 33	36%	74 < I < 77	66%	44 < I < 47	49%	68 < I < 74	75%	54 < I < 57	50%
Nb	14 < I < 16	47%	14 < I < 15	48%	17 < I < 21	72%	< LOD mix		< LOD mix		11 < I < 14	76%
Cs	3 < I < 3	50%	3 < I < 3	57%	17 < I < 18	66%	8 < I < 9	51%	< LOD mix		10 < I < 11	51%
Ba	765	32%	429	19%	648	54%	665	31%	666	44%	687	36%
La	19	42%	14	33%	22	66%	13	56%	< 14		13	55%
Ce	40	38%	30	23%	45	62%	25	43%	47	56%	31	45%
Nd	12	66%	9 < I < 11	80%	16	89%	17 < I < 21	73%	< LOD mix		11	82%
Pb	23	47%	16	43%	20	83%	13	75%	< 43		< 15	
Th	7 < I < 7	44%	4 < I < 4	47%	9 < I < 9	68%	4 < I < 5	61%	20 < I < 21	66%	6 < I < 6	57%
U	1 < I < 1	59%	< LOD mix		1 < I < 1	82%	1 < I < 1	89%	< LOD mix		1 < I < 1	85%
Size (μm)	14		9		13		7		10		15	
x	0.12		0.53		0.07		0.28		0.35		0.16	

	p18		p28		p29		p30		p31R		p32R	
SiO_2	73.47	11%	73.08	16%	73.60	44%	72.79	32%	74.23	15%	< 106.69	
TiO_2	0.02 < I < 0.03	68%	< LOD mix		< LOD mix		< LOD mix		< LOD mix		0.02 < I < 0.14	256%
Al_2O_3	14.12	11%	14.06	17%	13.97	66%	14.32	36%	14.08	19%	< 28.15	
Fe_2O_3	0.37	55%	< 0.49		< LOD mix		0.60 < I < 0.85	109%	< 0.35		1.48	235%
MnO	0.02	26%	< LOD mix		< LOD mix		< LOD mix		0.01	50%	0.19	241%
MgO	0.09 < I < 0.09	69%	< LOD mix		< LOD mix		< LOD mix		< LOD mix		-0.10 < I < 0.23	
CaO	< 2.04		< 3.52		< 10.29		< 7.00		< 2.74		ext. < 0	
Na_2O	3.38	11%	3.93	14%	5.18	29%	2.79	45%	4.05	15%	9.37	124%
K_2O	3.97	9%	2.59	13%	2.05	42%	4.08	29%	2.89	15%	16.28	236%
Total	95.34		93.66		94.80		93.97		95.25		27.30	
Cu	< LOD mix		< LOD mix		< LOD mix		< LOD mix		< LOD mix		< LOD mix	
Zn	< LOD mix		< LOD mix		< LOD mix		< LOD mix		< LOD mix		< LOD mix	
Rb	230 < I < 231	14%	125 < I < 127	24%	72 < I < 79	73%	186 < I < 191	41%	123 < I < 125	24%	763	244%
Sr	417	34%	788	26%	1273	43%	591	87%	642	36%	ext. < 0	
Y	11 < I < 11	39%	4 < I < 5	102%	< LOD mix		< LOD mix		< LOD mix		4 < I < 22	249%
Zr	61 < I < 62	28%	46 < I < 49	43%	37 < I < 43	103%	56 < I < 66	65%	41 < I < 43	42%	158 < I < 184	245%
Nb	12 < I < 13	59%	< LOD mix		< LOD mix		< LOD mix		14 < I < 16	60%	28 < I < 59	249%
Cs	15 < I < 15	27%	3 < I < 4	84%	< LOD mix		< LOD mix		7 < I < 7	50%	45 < I < 54	245%
Ba	363	18%	445	25%	< 312		422	50%	417	25%	< 914	
La	14	32%	15	43%	< 17		18	72%	5	81%	51	236%
Ce	21	26%	25	33%	< 18		33	56%	11	50%	78	235%

(continued on next page)

Table 6 (*continued*)

	p18		p28		p29		p30		p31R		p32R	
Nd	$10<I<12$	73%	<LOD mix		<LOD mix		<27		<LOD mix		<45	
Pb	18	41%	24	49%	<LOD mix		<29		15	63%	94	231%
Th	$5<I<5$	45%	$4<I<5$	65%	<LOD mix		$10<I<11$	73%	$4<I<4$	67%	$7<I<13$	249%
U	$2<I<2$	50%	$2<I<2$	87%	<LOD mix		<LOD mix		$1<I<2$	78%	<LOD mix	
Size (μm)	12		8		8		9		11		15	
x	0.65		0.55		0.24		0.39		0.50		0.02	

	p34		p38		p39		p52		p59		p61	
SiO_2	70.95	26%	73.04	10%	75.19	29%	70.54	28%	69.99	21%	71.55	10%
TiO_2	$0.05<I<0.06$	55%	$0.02<I<0.02$	41%	<LOD mix		<LOD mix		$0.01<I<0.02$	114%	$0.03<I<0.03$	37%
Al_2O_3	14.28	37%	14.22	11%	14.04	27%	14.05	36%	14.07	26%	14.04	12%
Fe_2O_3	0.62	50%	0.51	25%	<0.68		<0.38		0.31	73%	0.24	48%
MnO	0.02	43%	0.03	17%	<LOD mix		<0.01		0.01	67%	0.01	30%
MgO	<LOD mix		$0.02<I<0.04$	129%	<LOD mix		<LOD mix		$0.04<I<0.06$	185%	<LOD mix	
CaO	<3.43		<1.23		<6.38		<4.34		3.33	73%	2.33	51%
Na_2O	3.90	39%	4.16	12%	2.65	49%	5.65	24%	5.70	17%	4.69	10%
K_2O	4.80	32%	3.46	10%	2.95	21%	1.91	25%	2.53	20%	3.12	10%
Total	94.57		95.41		94.83		92.16		95.93		95.97	
Cu	<LOD mix		<LOD mix		<LOD mix		<LOD mix		<LOD mix		$22<I<28$	103%
Zn	$41<I<80$	161%	<LOD mix		<LOD mix		<LOD mix		<LOD mix		<LOD mix	
Rb	$238<I<240$	38%	211	13%	$122<I<126$	34%	88	41%	94	31%	$143<I<144$	15%
Sr	<377		214	62%	<377		642	99%	1030	39%	733	27%
Y	$4<I<5$	78%	$5<I<6$	38%	$9<I<11$	81%	$7<I<7$	82%	$6<I<7$	70%	$5<I<5$	44%
Zr	$85<I<88$	43%	$83<I<85$	19%	$18<I<23$	93%	$31<I<34$	62%	$37<I<39$	48%	$44<I<45$	26%
Nb	$14<I<17$	57%	$15<I<17$	31%	<LOD mix		$7<I<10$	106%	$8<I<10$	78%	$11<I<12$	44%
Cs	$17<I<18$	44%	$20<I<21$	18%	$9<I<11$	59%	$3<I<4$	86%	$6<I<7$	56%	$5<I<5$	35%
Ba	680	34%	324	16%	681	32%	258	59%	196	57%	877	12%
La	20	46%	11	26%	20	52%	9	75%	8	65%	11	28%
Ce	34	41%	20	21%	23	50%	11	70%	24	38%	17	24%
Nd	$16<I<20$	68%	$11<I<13$	48%	<20		<LOD mix		$10<I<13$	95%	$6<I<7$	81%
Pb	27	54%	21	28%	<24		<15		<12		13	40%
Th	$17<I<18$	45%	$11<I<12$	22%	$6<I<7$	73%	$2<I<2$	100%	$5<I<6$	55%	$3<I<4$	40%
U	$6<I<6$	49%	$5<I<6$	24%	$2<I<3$	88%	<LOD mix		$2<I<2$	71%	$1<I<1$	56%
Size (μm)	11		8		8		10		7		11	
x	0.26		0.48		0.33		0.29		0.35		0.52	

	p64R		p68		p69		p71		p72		p73R	
SiO_2	71.21	13%	71.94	8%	72.91	15%	72.43	7%	71.57	15%	72.65	83%
TiO_2	$0.02<I<0.02$	67%	$0.01<I<0.01$	51%	0.01	83%	$0.03<I<0.03$	25%	$0.02<I<0.02$	59%	$0.08<I<0.11$	119%
Al_2O_3	14.07	18%	14.03	9%	14.04	17%	14.14	6%	14.04	21%	<14.42	
Fe_2O_3	0.31	46%	0.22	37%	0.25	60%	0.41	18%	0.25	55%	<0.82	
MnO	0.02	27%	0.01	22%	0.01	36%	0.02	13%	0.01	35%	0.06	99%
MgO	$0.03<I<0.05$	108%	<LOD mix		<LOD mix		$0.04<I<0.04$	60%	$0.03<I<0.04$	117%	$0.03<I<0.17$	304%
CaO	2.23	74%	2.00	41%	<2.20		1.06	51%	2.29	72%	<10.49	
Na_2O	5.27	12%	5.36	6%	4.75	15%	3.92	8%	5.22	15%	ext. < 0	
K_2O	2.81	14%	2.43	7%	3.03	14%	3.94	6%	2.55	16%	9.09	92%
Total	95.93		95.99		95.01		95.93		95.94		81.80	
Cu	<LOD mix		<LOD mix		<LOD mix		<LOD mix		<LOD mix		$40<I<129$	139%
Zn	$47<I<68$	85%	<LOD mix		<LOD mix		$30<I<38$	59%	<LOD mix		<LOD mix	
Rb	$76<I<78$	21%	99	12%	119	21%	$191<I<191$	9%	103	24%	$437<I<448$	100%
Sr	779	39%	923	14%	699	39%	446	22%	791	41%	ext. < 0	

Table 6 (*continued*)

	p64R		p68		p69		p71		p72		p73R	
Y	$3<I<4$	66%	$4<I<4$	41%	$6<I<7$	50%	$7<I<7$	26%	$2<I<2$	93%	$20<I<26$	110%
Zr	46	29%	27	24%	$40<I<41$	35%	$62<I<63$	16%	$35<I<36$	37%	$96<I<109$	106%
Nb	$9<I<10$	50%	$6<I<6$	47%	$7<I<9$	69%	$11<I<11$	28%	$3<I<5$	79%	$24<I<34$	118%
Cs	$3<I<3$	45%	$2<I<2$	38%	$3<I<4$	51%	$4<I<4$	25%	$2<I<2$	64%	$13<I<16$	109%
Ba	245	31%	457	11%	482	21%	636	9%	525	21%	1463	88%
La	13	31%	8	26%	11	38%	16	16%	8	46%	54	101%
Ce	22	25%	17	18%	25	27%	32	12%	19	31%	67	100%
Nd	7	87%	$6<I<7$	61%	< LOD mix		$13<I<14$	33%	7	90%	$54<I<71$	115%
Pb	14	46%	16	25%	10	67%	17	20%	13	54%	< 44	
Th	$3<I<3$	49%	$2<I<2$	46%	$4<I<4$	49%	$5<I<6$	23%	$2<I<2$	64%	10	116%
U	< LOD mix		$0<I<1$	71%	< LOD mix		$1<I<1$	37%	< LOD mix		$3<I<5$	132%
Size (μm)	10		12		10		15		10		10	
x	0.40		0.60		0.39		0.71		0.40		0.08	

	p74		p75		p77		p78R		p79R		p87	
SiO_2	71.76	15%	71.92	12%	75.75	62%	71.67	11%	< 286.04		73.73	15%
TiO_2	$0.01<I<0.01$	123%	< LOD mix		$0.03<I<0.06$	119%	0.01	74%	< LOD mix		$0.01<I<0.02$	72%
Al_2O_3	14.05	19%	14.04	14%	14.25	75%	14.05	13%	< 28.28		14.10	20%
Fe_2O_3	0.25	61%	0.25	44%	< 0.67		0.27	36%	$0.28<I<5.69$	276%	0.33	48%
MnO	0.01	50%	0.01	26%	0.04	79%	0.02	17%	$0.02<I<0.27$	245%	0.02	28%
MgO	< LOD mix		$0.03<I<0.04$	68%	$0.06<I<0.18$	119%	$0.03<I<0.04$	72%	< LOD mix		< LOD mix	
CaO	< 2.13		1.98	67%	ext. < 0		1.91	61%	$-5.27<I<57.59$		< 2.25	
Na_2O	6.05	11%	5.43	11%	ext. < 0		5.45	10%	ext. < 0		4.00	20%
K_2O	2.19	14%	2.32	11%	9.38	69%	2.57	11%	14.55	185%	3.05	16%
Total	94.30		95.96		99.41		95.96		14.55		95.24	
Cu	< LOD mix		< LOD mix		< LOD mix		< LOD mix		< LOD mix		< LOD mix	
Zn	< LOD mix		< 42		< LOD mix		< LOD mix		< LOD mix		< LOD mix	
Rb	70	25%	89	17%	$519<I<528$	75%	104	16%	$832<I<1099$	200%	138	22%
Sr	869	30%	380	57%	< 1013		882	27%	< 2891		727	48%
Y	< LOD mix		< LOD mix		$11<I<14$	95%	$3<I<4$	44%	< LOD mix		$4<I<6$	50%
Zr	$18<I<20$	49%	$22<I<23$	30%	$112<I<129$	80%	$23<I<24$	29%	< LOD mix		$42<I<44$	32%
Nb	$7<I<8$	62%	$3<I<5$	63%	$29<I<40$	90%	$6<I<7$	47%	< LOD mix		$5<I<8$	62%
Cs	$5<I<5$	42%	$5<I<5$	29%	$28<I<31$	80%	$8<I<8$	25%	$-26<I<38$		$3<I<4$	46%
Ba	327	25%	150	35%	961	70%	612	14%	ext. < 0		635	19%
La	6	56%	4	56%	29	83%	12	26%	$18<I<106$	228%	15	33%
Ce	12	37%	8	35%	54	78%	23	20%	144	211%	26	26%
Nd	$5<I<7$	131%	< LOD mix		$14<I<26$	121%	6	69%	$-3<I<259$		$10<I<13$	57%
Pb	14	52%	17	34%	36	101%	19	28%	< LOD mix		21	41%
Th	$1<I<1$	109%	$4<I<5$	30%	$28<I<30$	80%	$2<I<2$	51%	$14<I<36$	249%	$5<I<5$	39%
U	$1<I<1$	85%	$2<I<2$	34%	$12<I<14$	81%	$1<I<1$	48%	< LOD mix		< LOD mix	
Size (μm)	10		11		9		12		6		10	
x	0.41		0.38		0.10		0.46		0.05		0.34	

	p88		p89		p90R		p91		p96		p100R	
SiO_2	71.97	10%	73.31	18%	74.81	15%	72.73	25%	77.81	37%	72.22	8%
TiO_2	$0.01<I<0.02$	44%	< 0.02		0.04	31%	< LOD mix		0.02	86%	$0.02<I<0.02$	41%
Al_2O_3	14.65	15%	14.15	22%	14.25	26%	13.99	28%	13.89	58%	14.06	9%
Fe_2O_3	0.35	27%	0.33	62%	0.60	27%	< 0.37		ext. < 0		0.28	30%
MnO	0.02	19%	0.01	48%	0.05	25%	< 0.01		0.03	55%	0.02	16%
MgO	0.03	99%	< LOD mix		0.08	50%	$0.06<I<0.07$	145%	ext. < 0		$0.03<I<0.03$	76%
CaO	< 1.08		< 2.87		ext. < 0		< 3.71		ext. < 0		1.98	42%

(continued on next page)

Table 6 (*continued*)

	p88		p89		p90R		p91R		p96R		p1007	
Na_2O	5.06	11%	3.14	33%	1.89	72%	4.69	28%	3.61	81%	4.48	7%
K_2O	3.05	12%	3.31	18%	4.58	22%	2.13	20%	4.83	48%	2.92	7%
Total	95.14		94.26		96.31		93.53		100.19		95.95	
Cu	<LOD mix		<LOD mix		<LOD mix		<LOD mix		<LOD mix		<LOD mix	
Zn	<LOD mix		<LOD mix		<40		<LOD mix		<67		<LOD mix	
Rb	124	16%	$148<I<151$	25%	192	26%	$91<I<94$	33%	229	57%	122	12%
Sr	665	42%	672	58%	<244		886	44%	ext.<0		523	20%
Y	$7<I<7$	29%	$7<I<8$	55%	9	31%	$4<I<5$	98%	$7<I<7$	69%	$3<I<3$	47%
Zr	$37<I<38$	23%	$34<I<38$	41%	$74<I<76$	27%	$25<I<28$	58%	42	62%	$39<I<40$	21%
Nb	$8<I<9$	34%	<LOD mix		$15<I<16$	32%	$7<I<10$	80%	8	81%	$9<I<10$	36%
Cs	$5<I<6$	26%	$3<I<4$	60%	$4<I<4$	33%	$8<I<8$	51%	13	61%	$10<I<10$	19%
Ba	602	14%	681	22%	959	20%	527	32%	344	51%	297	13%
La	16	22%	15	39%	18	27%	8	78%	10	66%	10	22%
Ce	30	18%	30	31%	32	25%	21	44%	14	62%	14	19%
Nd	11	41%	$12<I<15$	72%	11	44%	$17<I<20$	83%	$7<I<10$	100%	<3	
Pb	12	40%	18	56%	29	28%	<16		28	62%	18	23%
Th	$3<I<4$	31%	$2<I<3$	60%	$7<I<7$	30%	$3<I<4$	68%	$7<I<8$	63%	$6<I<6$	24%
U	$0<I<1$	54%	$0<I<1$	236%	$1<I<2$	34%	<LOD mix		$4<I<5$	63%	$3<I<3$	27%
Size (μm)	13		10		20		6		13		13	
x	0.46		0.37		0.20		0.27		0.10		0.61	

	p102		p104		p105		p106		p107R		p108	
SiO_2	73.44	32%	73.16	14%	71.18	27%	66.99	86%	135.31	60%	72.50	17%
TiO_2	<LOD mix		$0.01<I<0.02$	82%	<LOD mix		$0.03<I<0.14$	98%	$0.05<I<0.07$	100%	$0.02<I<0.02$	80%
Al_2O_3	13.89	37%	14.07	17%	15.52	13%	14.55	86%	13.88	91%	14.03	21%
Fe_2O_3	ext.<0		0.30	50%	3.16	23%	1.13	122%	ext.<0		<0.28	
MnO	0.02	74%	0.02	32%	<LOD mix		0.09	86%	ext.<0		0.01	42%
MgO	<LOD mix		<LOD mix		$0.66<I<0.70$	46%	<LOD mix		ext.<0		<LOD mix	
CaO	<5.70		<2.24		<6.26		ext.<0		ext.<0		<2.98	
Na_2O	3.96	41%	3.92	15%	1.36	57%	2.93	88%	4.58	52%	5.26	14%
K_2O	2.79	29%	3.00	14%	2.41	12%	11.75	79%	7.46	82%	2.74	16%
Total	94.10		94.46		93.64		97.43		161.24		94.55	
Cu	<LOD mix		<LOD mix		<LOD mix		<LOD mix		<LOD mix		<LOD mix	
Zn	<LOD mix		<LOD mix		<LOD mix		<LOD mix		<LOD mix		<LOD mix	
Rb	$148<I<152$	41%	$135<I<137$	20%	$144<I<146$	23%	578	82%	362	87%	$126<I<128$	24%
Sr	612	66%	413	53%	571	30%	ext.<0		ext.<0		765	43%
Y	<LOD mix		6	56%	<LOD mix		$-2<I<22$		ext.<0		$5<I<6$	71%
Zr	$54<I<57$	57%	$38<I<40$	32%	<LOD mix		$334<I<384$	85%	$162<I<169$	89%	39	39%
Nb	<LOD mix		$13<I<15$	49%	<LOD mix		$63<I<101$	91%	$30<I<36$	95%	$11<I<14$	57%
Cs	$7<I<8$	71%	$11<I<12$	29%	$5<I<6$	105%	$58<I<74$	85%	$30<I<31$	89%	$8<I<9$	41%
Ba	440	42%	346	21%	179	52%	508	87%	585	74%	351	27%
La	<8		9	42%	<7		52	88%	ext.<0		11	44%
Ce	<10		16	30%	13	56%	56	88%	ext.<0		16	37%
Nd	<LOD mix		$6<I<8$	80%	<LOD mix		<LOD mix		ext.<0		$8<I<11$	103%
Pb	39	60%	21	39%	29	62%	84	96%	47	85%	17	52%
Th	$3<I<4$	89%	5	41%	<LOD mix		$36<I<45$	87%	$21<I<22$	90%	$3<I<3$	59%
U	$3<I<4$	72%	$3<I<3$	40%	<LOD mix		$18<I<22$	91%	9	91%	$3<I<3$	44%
Size (μm)	8		10		15		14		19		15	
x	0.23		0.42		0.44		0.12		0.09		0.35	

	p110		p115R		p116		p117R		p118		p119R	
SiO_2	81.74	82%	81.02	42%	72.70	22%	71.89	38%	72.43	47%	69.89	17%
TiO_2	$0.04<I<0.08$	134%	0.05	82%	<0.01		0.04	84%	<LOD mix		<LOD mix	

Table 6 (*continued*)

	p110		p115R		p116		p117R		p118		p119R	
Al_2O_3	< 15.03		14.33	79%	14.03	33%	14.19	80%	14.02	64%	14.41	20%
Fe_2O_3	< 0.95		0.80	72%	< 0.24		0.57	71%	< 0.62		0.92	28%
MnO	0.03	122%	0.08	73%	0.03	37%	0.04	69%	0.03	69%	0.01	41%
MgO	< LOD mix		< 0.13		< LOD mix		0.07 < *I* < 0.11	117%	< 0.25		0.11	81%
CaO	ext. < 0		ext. < 0		< 2.97		< 5.06		< 7.79		< 2.65	
Na_2O	ext. < 0		ext. < 0		5.43	19%	3.59	66%	5.28	40%	6.12	12%
K_2O	6.86	100%	6.11	68%	2.94	26%	4.40	65%	2.61	50%	3.17	17%
Total	88.63		102.39		95.12		94.71		94.37		94.63	
Cu	< LOD mix		< LOD mix		< LOD mix		< LOD mix		< LOD mix		< LOD mix	
Zn	< LOD mix		< LOD mix		< LOD mix		< 86		< LOD mix		< LOD mix	
Rb	354 < *I* < 372	111%	381	75%	128 < *I* < 131	34%	195	73%	102	66%	89	23%
Sr	< 1497		ext. < 0		305	130%	693	134%	913	66%	727	29%
Y	7 < *I* < 15	134%	17 < *I* < 19	79%	2 < *I* < 2	123%	11 < *I* < 12	80%	< LOD mix		< LOD mix	
Zr	100 < *I* < 119	116%	162 < *I* < 168	76%	18 < *I* < 20	59%	72	76%	19 < *I* < 25	108%	37 < *I* < 39	33%
Nb	147 < *I* < 166	113%	27 < *I* < 31	79%	8 < *I* < 10	71%	18 < *I* < 22	80%	< LOD mix		8 < *I* < 10	60%
Cs	< LOD mix		32 < *I* < 33	76%	9 < *I* < 9	46%	14	76%	10 < *I* < 11	81%	< LOD mix	
Ba	1006	96%	1330	65%	307	33%	743	56%	551	57%	303	25%
La	< 20		26	72%	13	46%	16	71%	< 12		8	44%
Ce	31	117%	49	71%	14	46%	24	68%	< 13		17	31%
Nd	4 < *I* < 29	192%	< 13		< LOD mix		12	98%	< LOD mix		< LOD mix	
Pb	< 50		28	77%	19	57%	24	76%	< 31		19	47%
Th	15 < *I* < 19	119%	19 < *I* < 20	77%	4 < *I* < 5	60%	14 < *I* < 15	76%	< LOD mix		5 < *I* < 5	42%
U	6	137%	4	85%	2 < *I* < 3	61%	6 < *I* < 7	77%	< LOD mix		4 < *I* < 4	38%
Size (μm)	6		16		10		17		12		12	
x	0.08		0.07		0.32		0.10		0.15		0.30	

	p120R		p121R		p125		p126		p128		p134R	
SiO_2	72.07	11%	72.75	13%	< 726.38		71.99	15%	< 88.69		69.73	19%
TiO_2	0.01 < *I* < 0.01	69%	0.02 < *I* < 0.02	56%	0.38 < *I* < 0.71	822%	0.01	49%	0.13 < *I* < 0.17	128%	0.02 < *I* < 0.03	73%
Al_2O_3	14.13	16%	14.10	19%	< 147.61		14.00	26%	< 18.87		14.06	23%
Fe_2O_3	0.43	26%	0.36	34%	< 7.64		0.19	43%	1.37	125%	< 0.55	
MnO	0.03	18%	0.02	23%	0.22	810%	0.02	25%	0.09	119%	0.01	56%
MgO	0.05 < *I* < 0.06	75%	0.03 < *I* < 0.05	119%	< LOD mix		< 0.03		0.04 < *I* < 0.19	257%	< LOD mix	
CaO	< 1.25		< 1.55		< 96.38		< 1.51		< 12.48		< 4.07	
Na_2O	5.21	9%	5.32	11%	ext. < 0		6.67	12%	ext. < 0		5.74	16%
K_2O	3.03	13%	3.16	16%	80.67	813%	1.93	17%	13.19	115%	3.64	19%
Total	94.90		95.71		80.90		94.81		14.64		93.18	
Cu	< LOD mix		< LOD mix		< LOD mix		< LOD mix		178 < *I* < 269	147%	< LOD mix	
Zn	42 < *I* < 56	61%	< LOD mix		< LOD mix		ext. < 0		< LOD mix		< LOD mix	
Rb	139	18%	135	21%	4860 < *I* < 4980	820%	80	26%	710 < *I* < 721	121%	148 < *I* < 152	30%
Sr	476	42%	383	66%	ext. < 0		766	61%	ext. < 0		661	67%
Y	4	47%	8 < *I* < 8	39%	132 < *I* < 199	822%	3	40%	45 < *I* < 52	126%	6 < *I* < 8	89%
Zr	32 < *I* < 33	27%	51 < *I* < 52	28%	876 < *I* < 1039	821%	23 < *I* < 24	30%	303 < *I* < 316	123%	33 < *I* < 37	58%
Nb	14 < *I* < 15	32%	12 < *I* < 14	40%	264 < *I* < 385	822%	5 < *I* < 6	41%	41 < *I* < 62	131%	< LOD mix	
Cs	13 < *I* < 14	22%	9 < *I* < 10	29%	336 < *I* < 366	821%	6 < *I* < 6	29%	16 < *I* < 21	128%	4 < *I* < 5	75%
Ba	356	16%	501	18%	11761	801%	299	27%	1743	107%	739	26%
La	8	30%	9	35%	543	817%	6	41%	69	121%	32	35%
Ce	14	23%	18	26%	903	817%	13	28%	120	120%	108	27%
Nd	4 < *I* < 5	77%	8 < *I* < 9	62%	443 < *I* < 606	822%	< 3		< 38		83 < *I* < 88	53%
Pb	15	33%	16	37%	< 419		7	67%	< 51		29	49%

(continued on next page)

Table 6 (*continued*)

	p120R		p121R		p125		p126		p128		p134R	
Th	$5<I<5$	30%	$8<I<9$	31%	$63<I<86$	823%	$2<I<3$	36%	$13<I<16$	130%	$17<I<18$	44%
U	$4<I<4$	30%	$5<I<5$	32%	$17<I<31$	824%	$1<I<1$	38%	$5<I<7$	134%	$2<I<2$	116%
Size (μm)	14		11		9		14		10		8	
x	0.52		0.50		0.01		0.20		0.06		0.41	

	p137R		p138R	
SiO_2	72.45	46%	75.88	45%
TiO_2	$0.04<I<0.07$	100%	$0.03<I<0.05$	85%
Al_2O_3	14.34	48%	14.16	53%
Fe_2O_3	< 0.99		< 0.85	
MnO	$0.01<I<0.03$	76%	$0.02<I<0.03$	72%
MgO	< LOD mix		< LOD mix	
CaO	ext. < 0		ext. < 0	
Na_2O	< 3.02		ext. < 0	
K_2O	9.79	45%	12.19	50%
Total	96.59		102.22	
Cu	< LOD mix		< LOD mix	
Zn	< LOD mix		$1030<I<1297$	67%
Rb	$412<I<439$	51%	$630<I<652$	55%
Sr	ext. < 0		ext. < 0	
Y	$27<I<36$	73%	$2<I<9$	222%
Zr	$76<I<96$	64%	$126<I<142$	64%
Nb	$12<I<31$	69%	< LOD mix	
Cs	$8<I<15$	71%	$13<I<17$	72%
Ba	1469	46%	2037	50%
La	97	52%	50	60%
Ce	247	50%	65	58%
Nd	$153<I<174$	63%	$23<I<38$	149%
Pb	< 33		384	54%
Th	$37<I<41$	57%	$14<I<17$	76%
U	$2<I<5$	102%	$2<I<4$	102%
Size (μm)	12		12	
x	0.16		0.15	

$5.77<I<6.00$: bracketing values.
< 0.03: below detection limit.
ext. < 0: calculated concentration below zero.
< LOD mix: mix analyses below detection limit.
R: recystallized inclusions.

affected by the compositional zonation present in the crystal. (3) Systematic uncertainties on x. In our example, this effect alone cannot account for the scatter in some elements (e.g. K) if x is calculated over a reasonable range of aluminium concentrations. (4) Non-representative sampling during the ablation. This latter influence should be most significant for elements strongly enriched in particular phases of re-crystallised melt inclusions. Re-crystallised inclusions are identified by the letter "R" in Table 6, but no obvious increase in the scatter is associated with these analyses. This reinforces the conclusion by Pettke et al. (2000) who argued that representative sampling is likely for transient signals that were sequentially recorded by more than approximately 25 sweeps.

The relative importance of these four effects cannot be quantified and varies with each system under consideration. In the present example, we suspect that the zonation in the plagioclase and true compositional changes in the melt dominate the scatter, for instance in potassium. However, for most major elements and some trace elements the calculated uncertainties overlap with the average concentration, reflecting the accuracy of the analytical approach and the validity of the quantification methods and the uncertainty calculation.

8. Conclusions

This study presents laser-ablation ICP-MS as a new method for efficient and accurate analysis of major to trace elements in single melt inclusions enclosed in magmatic phenocrysts. The main advantage over other techniques is the possibility of quantifying the composition of entire inclusions, even if these are heterogeneous (crystallized), hosted in chemically complex minerals and not exposed to the sample surface. The technique does not require homogenisation of crystallised inclusions prior to analysis and therefore avoids potential systematic errors resulting from heating experiments. Glassy and devitrified inclusions of variable sizes in a single assemblage can be analysed together for comparison. This is essential for testing the representativity of inclusion results for actual melt compositions. Most importantly, the possibility to analyse crystallised inclusions avoids a likely sampling bias inherent to conventional studies, which are systematically restricted to glassy inclusions. LA-ICP-MS with modern laser-optical systems has the additional advantage that external calibration is essentially matrix-independent, which is a prerequisite for the quantitative uncertainty analysis presented here. The same principle of quantification, using signal deconvolution by internal standar disation, can be used to analyse any other solid or liquid inclusions trapped in a mineral, including mineral, sulphide melt or fluid inclusions.

Several quantification methods for single melt inclusion analyses were tested. All aim at determining an internal standard through which the amount of host, which is always ablated together with the inclusion, can be subtracted from the mixed LA-ICP-MS signal. The advantage of using an internal standard is that the amount of host mineral crystallized onto the inclusion wall is automatically accounted for, by addition of the appropriate quantity of host to the inclusion. Such a correction should, in principle, also be applied in other analytical techniques (EMP, SIMS, PIXE) used for analysing glassy inclusions, where crystallisation onto the inclusion wall has always occurred to some degree, but where the correction is more difficult to evaluate than with bulk ablation and internal standardisation.

Laser-ablation ICP-MS allows numerous analyses of individual inclusions in a co-genetic population in a short time, with an efficiency of up to 100 analyses per day. Quantification of uncertainties in the element concentration of numerous individual inclusions allows the calculation of accurate uncertainty-weighted means and associated uncertainties for the chemical composition of a population of cogenetic melt inclusions. This allows screening of artefacts (e.g. non representative sampling or inclusion-size dependent boundary-layer effects) and significantly reduces the overall uncertainty in geochemically meaningful results. The efficiency and versatility of LA-ICP-MS offers a wider range of geochemical and petrologic applications, including experimental studies and investigations of magma chamber evolution, magmatic-hydrothermal ore formation and volcanic processes.

Acknowledgements

The authors would like to thank Urs Menet, Bruno Rütsche and Tony Willy for continuing technical support, Heidi Wunderli-Allenspach for providing access to the confocal microscope facility and Vladim Kamenetsky for a constructive review of the mauscript. We would also like to thank Detlef Günther for additional comments on the final version of this paper and particularly Felix Oberli whose help was essential for an accurate determination of the uncertainties.

References

Audétat, A., 1999. The magmatic-hydrothermal evolution of the Sn/W-mineralized Mole granite (Eastern Australia). PhD Thesis No. 13168, ETHZ, Zürich, 211 pp.

Audétat, A., Günther, D., Heinrich, C.A., 1998. Formation of a magmatic-hydrothermal ore deposit: Insights with LA-ICP-MS analysis of fluid inclusions. Science 279 (5359), 2091–2094.

Audétat, A., Günther, D., Heinrich, C.A., 2000. Magmatic-hydrothermal evolution in a fractionating granite: a microchemical study of the Sn-W-F-mineralized Mole Granite (Australia). Geochimica et Cosmochimica Acta 64 (19), 3373–3393.

Bevington, P.R., Robinson, D.K., 1992. Data Reduction and Uncertainty Analysis for the Physical Sciences, 2nd edn. McGraw-Hill, New York, 328 pp.

Clocchiatti, R., 1975. Les inclusions vitreuses des cristaux de quartz.

Etude optique, thermoptique et chimique. Applications géologiques. Mémoires de la Société de Géologie 122, 1–96.

Dietrich, A., Lehmann, B., Wallianos, A., 2000. Bulk rock and melt inclusion geochemistry of Bolivian tin porphyry systems. Economic Geology and the Bulletin of the Society of Economic Geologists 95 (2), 313–326.

Fryer, B.J., Jackson, S.E., Longerich, H.P., 1995. Design, operation and role of the laser-ablation microprobe coupled with an inductively-coupled plasma-mass-spectrometer (Lam-Icp-Ms) in the Earth-Sciences. Canadian Mineralogist 33, 303–312.

Günther, D., Heinrich, C.A., 1999. Enhanced sensitivity in laser ablation-ICP mass spectrometry using helium–argon mixtures as aerosol carrier — plenary lecture. Journal of Analytical Atomic Spectrometry 14 (9), 1363–1368.

Günther, D., Frischknecht, R., Heinrich, C.A., Kahlert, H.J., 1997. Capabilities of an Argon Fluoride 193 nm excimer laser for laser ablation inductively coupled plasma mass spectrometry microanalysis of geological materials. Journal of Analytical Atomic Spectrometry 12 (9), 939–944.

Günther, D., Audétat, A., Frischknecht, R., Heinrich, C.A., 1998. Quantitative analysis of major, minor and trace elements in fluid inclusions using laser ablation inductively coupled plasma mass spectrometry. Journal of Analytical Atomic Spectrometry 13 (4), 263–270.

Kamenetsky, V.S., Eggins, S.M., Crawford, A.J., Green, D.H., Gasparon, M., Falloon, T.J., 1998. Calcic melt inclusions in primitive olivine at 43 degrees N MAR: evidence for melt–rock reaction/melting involving clinopyroxene-rich lithologies during MORB generation. Earth and Planetary Science Letters 160 (1–2), 115–132.

Kamenetsky, V.S., Wolfe, R.C., Eggins, S.M., Mernagh, T.P., Bastrakov, E., 1999. Volatile exsolution at the Dinkidi Cu–Au porphyry deposit, Philippines: a melt-inclusion record of the initial ore-forming process. Geology 27 (8), 691–694.

Lahaye, Y., Lambert, D., Walters, S., 1997. Ultraviolet laser sampling and high resolution inductively coupled plasma mass spectrometry of NIST and BCR-2G glass reference materials. Geostandards Newsletter — Journal of Geostandards and Geoanalysis 21 (2), 205–214.

Leach, A.M., Hieftje, G.M., 2000. Methods for shot-to-shot normalization in laser ablation with an inductively coupled plasma time-of-flight mass spectrometer. Journal of Analytical Atomic Spectrometry 15 (9), 1121–1124.

Longerich, H.P., Jackson, S.E., Günther, D., 1996. Laser ablation inductively coupled plasma mass spectrometric transient signal data acquisition and analyte concentration calculation. Journal of Analytical Atomic Spectrometry 11 (9), 899–904.

Lowenstern, J.B., 1995. Applications of silicate melt inclusions to the study15 of magmatic volatiles. In: Thompson, J.F.H. (Ed.), Magmas, Fluids and Ore Deposits. Mineralogical Association of Canada, Short Course, vol. 23, pp. 71–99.

Pearce, N.J.G., Perkins, W.T., Westgate, J.A., Gorton, M.P., Jackson, S.E., Neal, C.R., Chernery, S.P., 1997. A compilation of new and published major and trace element data for NIST SRM 610 and NIST SRM 612 glass reference materials. Geostandards Newsletter — Journal of Geostandards and Geoanalysis 21 (1), 115–144.

Pettke, T., Heinrich, C.A., Ciocan, A.C., Günther, D., 2000. Quadrupole mass spectrometry and optical emission spectroscopy: detection capabilities and representative sampling of short transient signals from laser-ablation. Journal of Analytical Atomic Spectrometry 15 (9), 1149–1155.

Sasso, A.M., 1997. Geological evolution and metallogenetic relationships of the Farallon Negro volcanic complex, NW Argentina. PhD Thesis, Queen's University. Kingston, Ontario, Canada, 842 pp.

Sobolev, A.V., Shimizu, N., 1993. Ultra-depleted primary melt included in an olivine from the mid-Atlantic ridge. Nature 363 (6425), 151–154.

Taylor, R.P., Jackson, S.E., Longerich, H.P., Webster, J.D., 1997. In situ trace-element analysis of individual silicate melt inclusions by laser ablation microprobe inductively coupled plasma-mass spectrometry (LAM-ICP-MS). Geochimica et Cosmochimica Acta 61 (13), 2559–2567.

Ulrich, T., 1999. Genesis of the Bajo de la Alumbrera porphyry Cu–Au deposit, Argentina: Geological, fluid geochemical, and isotopic implications. PhD Thesis No. 13383, ETHZ, Zürich, 207 pp.

Ulrich, T., Günther, D., Heinrich, C.A., 1999. Gold concentrations of magmatic brines and the metal budget of porphyry copper deposits. Nature 399 (6737), 676–679.

Webster, J.D., Duffield, W.A., 1991. Volatiles and lithophile elements in Taylor Creek Rhyolite — constraints from glass inclusion analysis. American Mineralogist 76 (9–10), 1628–1645.

Webster, J.D., Duffield, W.A., 1994. Extreme halogen abundances in tin-rich magma of the Taylor Creek Rhyolite, New-Mexico. Economic Geology and the Bulletin of the Society of Economic Geologists 89 (4), 840–850.